Glycolysis Induced by METTL14 Is Essential for Macrophage Phagocytosis and Phenotype in Cervical Cancer

Bingyu Wang,* Zhonghao Mao,* Jinwen Ye,* Xinlin Jiao,* Teng Zhang,* Qi Wang,*,† Sai Han,* Youzhong Zhang,* Chunling Wang,* Taotao Dong,* and Baoxia Cui*

N*^{6}-methyladenosine (m6A) is the most abundant mRNA modification in mammals and it plays a vital role in various biological processes. However, the roles of m6A on cervical cancer tumorigenesis, especially macrophages infiltrated in the tumor microenvironment of cervical cancer, are still unclear. We analyzed the abnormal m6A methylation in cervical cancer, using CaSki and THP-1 cell lines, that might influence macrophage polarization and/or function in the tumor microenvironment. In addition, C57BL/6J and BALB/c nude mice were used for validation in vivo. In this study, m6A methylated RNA immunoprecipitation sequencing analysis revealed the m6A profiles in cervical cancer. Then, we discovered that the high expression of METTL14 (methyltransferase 14, *N*^{6}-adenosine-methyltransferase subunit) in cervical cancer tissues can promote the proportion of programmed cell death protein 1 (PD-1)–positive tumor-associated macrophages, which have an obstacle to devour tumor cells. Functionally, changes of METTL14 in cervical cancer inhibit the recognition and phagocytosis of macrophages to tumor cells. Mechanistically, the abnormality of METTL14 could target the glycolysis of tumors in vivo and vitro. Moreover, lactate acid produced by tumor glycolysis has an important role in the PD-1 expression of tumor-associated macrophages as a proinflammatory and immunosuppressive mediator. In this study, we revealed the effect of glycolysis regulated by METTL14 on the expression of PD-1 and phagocytosis of macrophages, which showed that METTL14 was a potential therapeutic target for treating advanced human cancers.** ***The Journal of Immunology**, 2024, 212: 723–736.**

Cervical cancer is the fourth most diagnosed cancer and the fourth leading cause of cancer-associated mortality in women worldwide (1). In recent years, the acknowledgment of human papillomavirus as the primary cause of cervical cancer has led to further understanding of cervical cancer tumorigenesis. However, human papillomavirus infection is a necessary condition but not a sufficient condition (2, 3). Accumulating evidence has revealed that cervical cancer tumorigenesis is a multistep process involving the complicated interaction of transcriptomic alterations, genetics, and epigenetics. In particular, the molecular mechanisms related to the regulation of RNA *N*^{6}-methyladenosine (m6A) modification are interesting candidates.

m6A is the most abundant mRNA modification in mammals. It has been reported that METTL14 (methyltransferase 14, *N*^{6}-adenosine-methyltransferase subunit), as a subunit of methyltransferases, plays a role in a variety of diseases, particularly tumors (4–8). Previous studies have shown that m6A transferase levels are high in cervical cancer (9, 10). An increase in m6A methylation can lead to the invasion and migration of tumor cells and can be an indicator of poor clinical prognosis in human cancer patients (10–12). Additionally, m6A modification has also been associated with immune regulation: a recent study found that m6A-modified lysosomal cathepsin mRNAs are recognized by YTHDF1 in dendritic cells, subsequently accelerating the translation of cathepsins and shortening the duration of survival (13). $CD4^+$ T cells are primarily regulated by m6A to maintain naive T cell homeostasis (14). However, our understanding of the regulation of m6A modifications and expression of methyltransferase in cervical cancer on macrophages is still in its infancy.

In the immunosuppressive tumor microenvironment (TME), tumor-associated macrophages (TAMs) are prominent immune cells that play a crucial role in tumorigenesis. In general, they are skewed away from M1-like macrophages and toward M2-like macrophage properties (15–18). Programmed cell death protein 1 (PD-1) is an immune checkpoint receptor that is upregulated on activated T cells to induce immune

*Department of Obstetrics and Gynecology, Qilu Hospital of Shandong University, Jinan, People's Republic of China; and †Department of Obstetrics and Gynecology, The First Affiliated Hospital of Shandong First Medical University, Jinan, People's Republic of China

ORCIDs: 0000-0001-9678-912X (C.W.); 0000-0001-9088-1240 (B.C.).

Received for publication May 16, 2023. Accepted for publication October 3, 2023.

This work was supported by National Key Technology Research and Developmental Program of China Grants 2022YFC2704401 and 2021YFC2701200, the National Natural Science Foundation of China Grants 82172940 and 82103425, Natural Science Foundation of Shandong Province Grants ZR2021QH187 and ZR2021QH044, and by the Jinan City "20 New University" independent innovation group Grant 2021GXRC027. The study involving animals (Grant DWLL-2023-030) and humans (Grant KYLL-202111-153) was approved by the Ethics Committee of the Qilu Hospital of Shandong University.

B.W. and B.C. were responsible for the overall conception and design of the study and performed most of the experiments; J.Y. and Z.M. performed part of the experiments and the data analysis; X.J., T.Z., and Q.W. collected the samples and the data; S.H. coordinated the experiments; and Y.Z., C.W., and T.D. revised the manuscript. All authors reviewed, edited, and approved the manuscript.

The MeRIP-seq data presented in this article have been submitted to the Gene Expression Omnibus (https://www.ncbi.nlm.nih.gov/geo/query/acc.cgi?acc=GSE242071) under accession number GSE242071.

Address correspondence and reprint requests to Dr. Baoxia Cui, Department of Obstetrics and Gynecology, Qilu Hospital, Shandong University, 107 West Wenhua Road, Ji'nan, 250012 Shandong, People's Republic of China. E-mail address: cuibaoxia@sdu.edu.cn

The online version of this article contains supplemental material.

Abbreviations used in this article: AMPK, AMP-activated protein kinase; CDS, coding sequence; 2-DG, 2-deoxy-D-glucose; ECAR, extracellular acidification rate; EdU, 5-ethynyl-2′-deoxyuridine; HK2, hexokinase 2; m6a, *N*^{6}-methyladenosine; MeRIP, methylated RNA immunoprecipitation; MeRIP-seq, MeRIP sequencing; METTL14, methyltransferase 14, *N*^{6}-adenosine-methyltransferase subunit; NC, negative control; OCR, oxygen consumption rate; OXPHOS, oxidative phosphorylation; PD-1, programmed cell death protein 1; PKM2, M2 pyruvate kinase; PVDF, polyvinylidene difluoride; qPCR, quantitative PCR; shMETTL14, shRNA METTL14; sh-NC, shRNA NC; shRNA, short hairpin RNA; siGPR81, siRNA GPR81; siRNA, small interfering RNA; TAM, tumor-associated macrophage; TME, tumor microenvironment; UTR, untranslated region.

https://doi.org/10.4049/jimmunol.2300339

tolerance (19–22). Although most studies indicate that anti–PD-1 may cure cancer by activating tumor killing of T cells, recent theories suggest that PD-1 activation can also inhibit the antitumor activity of macrophages. Studies have shown that a large number of M2 macrophages express PD-1 (23). PD-1 expression in M2 macrophages is negatively correlated with phagocytic potency against tumor cells, and blockade of PD-1 in vivo increases macrophage phagocytosis and reduces tumor growth (24). The factors responsible for establishing and maintaining the macrophage polarization and PD-1 expression are beginning to emerge. In this study, we revealed that the expression of METTL14 in cervical cancer, as one of the key molecules regulating m6A methylation, contributes to the phenotype and function of macrophages. The molecular basis remains unclear.

Lactic acid is a metabolic product produced from glucose through glycolysis and the conversion of pyruvate by lactate dehydrogenase under oxygen deprivation conditions (25, 26). Lactic acid represents a crucial microenvironmental stressor that controls a number of immunosuppressive phenomena related to tumor progression (27–29). Studies have shown that tumor-derived lactate was shown to induce an M2-like polarization of both THP-1 human monocytic cells and LPS-activated human monocytes (30–32). Glycolysis, especially lactic acid production, is regarded to be a promising therapeutic mechanism in functions of TAMs (28, 30).

In this study, we found that METTL14 can mediate tumor glycolysis and lead to the accumulation of lactic acid in the TME. A large amount of lactic acid acts on the surface of macrophages, resulting in changes in the phenotype and function of macrophages, leading to immune escape. Taken together, our data suggest an important interplay between METTL14 and expression of PD-1 in TAMs through endogenous metabolic dysregulation, raising the possibility of developing new therapeutic strategies and targets for cervical cancer.

Materials and Methods

Patients and tissue samples

This study collected 20 cases of tissues, including cervical cancer tissues and paracarcinoma normal tissues from the same patients. These tissues were collected from cervical cancer patients at the Qilu Hospital of Shandong University from 2020 to 2022. The female patients were diagnosed with cervical cancer on a pathological basis. Inclusion criteria were newly treated patients with FIGO IB–IIA stage (regardless of histological type), the patient was ≥18 y of age, and the original treatment plan included radical resection of cervical cancer. Exclusion criteria included a history of pelvic lymph node resection or radiotherapy, abnormal liver and kidney function, and other clear contraindications to surgery. In this study, all experiments were approved by the Ethics Committee of the Qilu Hospital of Shandong University. The patients and their families were informed of specimen collection, and informed consent forms were signed.

Immunohistochemistry

Tissue sections were cut into 4.0-mm-thick slices and baked at 65°C for 65 min. Slices were deparaffinized twice in xylene for 15 min, dehydrated in 95, 80, and 70% ethanol, and then repaired in sodium citrate Ag retrieval solution heated to 96°C for 15 min. After 15 min at room temperature, 3% hydrogen peroxide in methanol was used to purge endogenous peroxide activity. FBS was used to block the sections for 45 min, after which they were incubated with the anti-METTL14 Ab (Abcam, catalog no. ab220030, RRID:AB_2893210, 1:300), anti–M2 pyruvate kinase (PKM2) Ab (Abcam, catalog no. ab85555, RRID:AB_10562282, 1:500), anti–hexokinase 2 (HK2) Ab (Abcam, catalog no. ab209847, RRID:AB_2904621, 1:500), and the anti–AMP-activated protein kinase (AMPK) Ab (Abcam, catalog no. ab32047, RRID:AB_722764, 1:200) overnight (~19 h) at 4°C. Following this, the secondary Ab was incubated at room temperature for 60 min (~28°C). Diaminobenzidine was used to incubate the tissue slices. As a final step, the slices were stained with hematoxylin, made transparent with gradient alcohol solution and xylene solution, and then dehydrated with neutral balsam. On the third day, images were captured under the microscope. Every experiment was repeated at least three times.

Methylated RNA immunoprecipitation sequencing and methylated RNA immunoprecipitation–quantitative PCR assays

For methylated RNA immunoprecipitation (MeRIP) sequencing (MeRIP-seq), total RNA was isolated. A Dynabeads mRNA DIRECT kit (Thermo Fisher Scientific) was used to purify mRNA and fragment it by sonication, followed by MeRIP-seq and library preparation. To prepare libraries, we used the TruSeq stranded mRNA library prep kit (Illumina, San Diego, CA) to purify mRNA fragments. Sequencing was carried out on the Illumina HiSeq 2000 system with a pair-end 150-bp read length. Reads were aligned to human genome version 38 (GRCh38) with TopHat. When a gene had more than one isoform, the longest isoform was retained. Different m6A-modified peaks were identified between IP and input samples using the software exomePeak ($p < 0.01$).

A MeRIP–quantitative PCR (qPCR) assay was performed as the m6A MeRIP kit instructions mention (Bersinbio, catalog no. 5203-2). Total RNA was extracted from CaSki cells and then conjugated with anti-m6A Ab and anti-IgG in IP buffer. Precipitated m6A-modified AMPK levels were calculated from the $2^{-\Delta\Delta Ct}$ compared with the input sample.

Immunofluorescence staining

For PD-1, CD206, and γ-H2AX staining, histological sections and cells were blocked with 10% FBS (Life Technologies, Carlsbad, CA) and were stained with anti–PD-1 Ab (Abcam, catalog no. ab52587, RRID:AB_881954, 1:250; CST, catalog no. 84651, RRID:AB_2800041), anti-CD206 Ab (Abcam, catalog no. ab64693, RRID:AB_1523910, 1:200), and the γ-H2AX Ab (Abcam, catalog no. ab81299, RRID:AB_1640564, 1:300). DyLight 488 goat anti-rabbit IgG (Abbkine, catalog no. A23220, RRID:AB_2737289) and DyLight 594 goat anti-mouse IgG (Abbkine, catalog no. A23410) were used as secondary Abs. A fluorescence microscope was used to observe experimental results. We used Image-Pro Plus 6.0 software to select both red and green areas as the unified standard for determining the positivity of all images and calculate the average fluorescence intensity of the positive area in each image. Then, we calculated p values using a t test. For experiments, we randomly selected three fields of view for each experiment to calculate the average fluorescence intensity and took the average value.

Total protein extraction and Western blot

Total protein of cells or tissues was extracted using 500 μl of RIPA buffer with 1% PMSF. A bicinchoninic acid protein assay kit was used to measure the protein concentrations (40 g per sample), and SDS loading buffer was used to create the protein supernatant. In this study, a protein sample was separated by SDS-PAGE gel electrophoresis and then transferred to polyvinylidene difluoride (PVDF) membranes (0.22 or 0.45 mm) by electrophoresis. After that, the PVDF membranes containing protein were blocked with 5% skimmed milk powder at room temperature (~28°C). Then, we put the PVDF membranes into diluted primary Abs (diluted by Western primary Ab dilution buffer, Beyotime, Shanghai, China) anti-METTL14 Ab (Abcam, catalog no. ab220030, RRID:AB_2893210, 1:1000), anti-PKM2 Ab (Abcam, catalog no. ab85555, RRID:AB_10562282, 1:1000), anti-HK2 Ab (Abcam, catalog no. ab209847, RRID:AB_2904621, 1:1000), and the anti-AMPKα Ab (Abcam, catalog no. ab32047, RRID:AB_722764, 1:1000) at 4°C overnight, incubated with diluted secondary Abs (diluted by TBST) HRP-conjugated AffiniPure goat anti-mouse IgG (H+L) (Proteintech, Wuhan, China, SA00001-1, 1:5000) and HRP-conjugated AffiniPure goat anti-rabbit IgG (H+L) (Proteintech, Wuhan, China, SA00001-2, 1:5000), and detected the expression by an HRP chemiluminescence detection kit (Immobilon Western chemiluminescent HRP substrate, MilliporeSigma, Burlington, MA, catalog no. WBKLS0100). Every experiment was repeated at least three times.

RNA extraction and quantitative real-time PCR

TRIzol (Ambion, Life Technologies, Carlsbad, CA) was used to extract the total RNA of tissues and cells, and the concentration of each RNA sample was tested. The RNA was reversed into cDNA with a reverse transcription kit. Then, we amplified the aimed gene fragment and detected it with a SYBR Green qPCR kit (Toyobo, Osaka, Japan); quantitative real-time PCR was performed for 40 cycles. All experiments were conducted at least three times. Relative gene expression levels were analyzed by the $2^{-\Delta\Delta Ct}$ method. PCR sequences used are as follows (forward/reverse): METTL14, 5′-CCTCCCATGTACTTACAAGCC-3′, 5′-TAGCAGTGCCAGTTTCTC-3′; AMPK, 5′-GGAGCCTTGATGTGGTAGGAA-3′, 5′-TCAAATAGCTCTCCTCCTGAGAC-3′; GPR81, 5′-TGGAGAACCATCTCTGCGTG-3′, 5′-ATAAGATGATGCCCGAGGGGC-3′; IL-10, 5′-TGCTGGACTTTAAGGGTTAC-3′, 5′-GTTCTCAGCTTGGGGCATCA-3′; TGF-β, 5′-ATGGAGAGAGGACTGCGGAT-3′, 5′-TAGTGTTCCCCACTGGTCCC-3′; HK2, 5′-TTCCCCTGCCACCAGACTAA-3′, 5′-TCAAAGTCCCCTCTCCTCTGG-3′; PKM2, 5′-ATGTCGAAGCCCCATAGTGAA-3′, 5′-TGGGTG

GTGAATCAATGTCCA-3′; β-actin, 5′-CATGTACGTTGCTATCCAGGC-3′, 5′-CTCCTTAATGTCACGCACGAT-3′; METTL14 (mouse), 5′-CTGAGAGTGCGGATAGCATTG-3′, 5′-GAGCAGATGTATCATAGGAAGCC-3′.

Cell culture and CaSki cells cocultured with macrophages

CaSki cells (cervical cancer cells) and THP-1 cells (acute monocytic leukemia) were cultured in RPMI 1640 medium (Gibco, Thermo Fisher Scientific, Waltham, MA) containing with 10% FBS (Life Technologies, Carlsbad, CA) and 1% penicillin-streptomycin (100×) (Solarbio, Beijing, China) at 37°C with 5% CO_2 atmosphere. TC-1 cells are mouse lung epithelial cells stably transfected with E6/E7. TC-1 cells are commonly used to construct animal models of cervical cancer. TC-1 was cultivated in DMEM medium (Life Technologies, Carlsbad, CA) containing 10% FBS (Life Technologies, Carlsbad, CA) and 1% penicillin-streptomycin (100×) (Solarbio, Beijing, China) at 37°C in a humidified 5% CO_2 incubator. The glycolysis inhibitor 2-deoxy-D-glucose (2-DG) (8 mM, 12 h, MedChemExpress, Beijing, China) was used to act on CaSki cervical cancer cells to build a glycolysis inhibition model. Dorsomorphin (compound C) is a selective and ATP-competitive AMPK inhibitor. Dorsomorphin (compound C) (10 μM, 18 h, MedChemExpress, Beijing, China) reduced AMPK phosphorylation levels in CaSki cells. THP-1–derived macrophages were obtained after treated with phorbol ester (PMA, Sigma-Aldrich, St. Louis, MO) (50 ng/ml) for 48 h. Then, cells were stimulated with 10 ng/ml IL-4 (R&D Systems, Minneapolis, MN) and 10 ng/ml IL-13 (R&D Systems, Minneapolis, MN) to M2 polarization. CaSki cells were cocultured with THP-1–derived M2 macrophages using a Transwell insert (0.4 μm; Corning, Corning, NY). Each lower well of plates was plated with ∼10,000 CaSki cells, and the upper well of plates was plated with ∼5000 THP-1–derived M2 macrophages.

Metabolomics

The cells of the short hairpin RNA (shRNA) METTL14 (shMETTL14) group ($n = 10$) and the negative control (NC) group ($n = 10$) were mixed with 80% acetonitrile, ground and centrifuged, and the supernatant was taken out for further experiments. Then, 100 μl of 3-nitrophenylhydrazine (200 mM, containing internal standard 40 ng/ml malic acid-d3) and 100 μl of EDC (*N*-(3-dimethylaminopropyl)-*N*′-ethylcarbodiimide hydrochloride) (120 mM; containing 6% pyridine) were added to the supernatant and vortexed for 1 min at 40°C for 1 h. Next, after centrifuging for 15 min, the supernatant was passed through a 0.22-μm filter membrane, diluted three times with 80% acetonitrile water (including 10 ng/ml of the internal standard after derivatization), and injected into the machine for liquid chromatography–tandem mass spectrometry analysis.

shRNAs, small interfering RNA, and genetic knockout

Plasmids expressing shRNA targeting METTL14 or scramble sequences were purchased from GeneChem. shRNA sequences were packed into a lentivirus packaging construct and transfected into CaSki cells with Lipofectamine 2000 (Invitrogen). CaSki cells were infected with shRNA-expressing lentiviruses and selected with 10 mg/ml puromycin. Small interfering RNA (siRNA) targeting GPR81 (siGPR81) was transfected into macrophages derived from THP-1 with Lipofectamine 3000 (Invitrogen). The sequences of siRNA GPR81 are as follows (forward/reverse): 5′-S GUGCUAGACUCUUUUCCUTT-3′, 5′-AS AGGAAAUAGAGUCUAGCAGTT-3′.

The sequences of shRNA are shown in Supplemental Table I.

Cell migration assay

Standard transwell inserts (0.8 μm; Corning, Corning, NY) were used to detect cell migration. CaSki cells were plated into the upper compartment with 500 μl of serum-free medium, and the lower compartment was filled with medium containing 10% FBS. After 24–48 h of incubation at 37°C, cotton swabs were used to remove the noninvaded cells on the filter's upper surface, and the cells were fixed for 2 min in 100% methanol. Invaded cells on the lower side of the filter were stained with 0.5% crystal violet for 20 min, and images were captured using a microscope.

Cell Counting Kit-8 assay

The Cell Counting Kit-8 assay kit (Beyotime, Shanghai, China) was used to evaluate the level of cell proliferation. Briefly, 10 μl of Cell Counting Kit solution was added to the culture medium and incubated for an additional 3 h. The absorbance was determined at 450-nm wavelength with a reference wavelength of 630 nm.

Lactic acid production, extracellular acidification rate, and oxygen consumption rate

Extracellular acidification rate (ECAR) and oxygen consumption rate (OCR) were analyzed using the Seahorse XF96 instruments (Seahorse Bioscience, Billerica, MA). For the OCR and ECAR tests, an assay medium (Seahorse Bioscience) containing 1 mM pyruvate, 10 mM glucose, and 2 mM glutamine was replaced with the cell medium for 1.5 h at 37°C. Rotenone/antimycin A (1.0 μm) and 2-DG (0.5 μm) were added to the system respectively, then measured by a glycolytic stress test kit (Seahorse Bioscience). The OCR and ECAR results were adjusted to the Seahorse XF96 Wave software. The lactate concentration in cultured media was measured using a lactate assay kit (Solarbio, Beijing, China) following the manufacturer's instructions.

Flow cytometry

Macrophages derived from THP-1 cells were collected and evaluated by flow cytometry. THP-1–derived macrophages were stained with the following fluorochrome-labeled Abs for 30 min at 4°C: anti-CD206 (BD Biosciences, San Jose, CA), anti-CD163 (R&D Systems, Minneapolis, MN), and anti–PD-1 (BD Biosciences, San Jose, CA). After the surface staining, these cell samples were detected using CytoFLEX, and the data were analyzed using CytExpert software. During the data analysis process, the cell populations of $CD163^+CD206^+$ were gated and the expression of PD-1 was statistically analyzed in the gated cell populations.

All staining was performed according to the manufacturer's protocols. The negative group without Abs was used for gating, and single-color stain controls were used to enable correct compensation (Supplemental Fig. 3C).

Phagocytosis assay

As shown in Supplemental Fig. 1A, THP-1–derived macrophages were cocultured with CaSki cells for 24 h. Macrophages and CaSki cells were digested with trypsin and stained with a Dil or Dio kit, respectively (Beyotime, Shanghai, China). Then, macrophages were plated at a density of 5×10^4 cells per well in a 24-well tissue culture plate and 2×10^5 CaSki cells were added after staining. The cocultured cells were incubated in serum-free medium for another 3 h and then analyzed by flow cytometer and imaged with a fluorescence microscope. In this experiment, macrophages expressed green fluorescence, whereas tumor cells expressed red fluorescence. Meanwhile, macrophages that simultaneously expressed red and green fluorescence were those that had devoured tumor cells. The proportion of double-positive cells in total cells is the phagocytic efficiency of macrophages.

The negative group without Abs was used for gating, and single-color stain controls were used to enable correct compensation (Supplemental Fig. 3D).

In vivo studies

BALB/c nude mice and C57BL/6J mice were purchased from GemPharmatech (Nanjing, China). Animal studies were performed according to institutional guidelines, and all experiments in this study were approved by the Ethics Committee of the Qilu Hospital of Shandong University. CaSki cells were transfected with shRNA NC (sh-NC) ($n = 6$) or shMETTL14 ($n = 6$). A total of 1×10^6 viable cells were injected into the right flanks of BALB/c nude mice. TC-1 cells were stably transfected with sh-NC ($n = 6$) or shMETTL14 shRNA ($n = 6$). A total of 5×10^6 viable cells were injected into the right flanks of C57BL/6J mice. Dorsomorphin was i.p. injected into mice to inhibit the expression of AMPK. The injection volume was 1 or 10 mg/kg. Then, after 12 d, mice were sacrificed, the tumors were dissected, and tumor weights were measured. Tumor sizes were measured using a Vernier caliper, and the tumor volume was calculated using the following formula: $\text{volume} = {}^1/_2 \times \text{length} \times \text{width}^2$.

5-Ethynyl-2′-deoxyuridine incorporation assay

A Cell Light 5-Ethynyl-2′-deoxyuridine (EdU) Apollo 567 cell kit (RiboBio, Guangzhou, China) was used to detect the newly synthesized DNA and cell proliferation according to the manufacturer's directions. EdU-positive cells were manually counted as percentages of cells calculated by the DAPI nuclear label.

ELISA assay

A human IL-10 Quantikine ELISA kit (MultiSciences Biotech, Hangzhou, China) and human TGF-β Quantikine ELISA kit (MultiSciences Biotech, Hangzhou, China) were used to detect the content of cytokines in culture supernatant collected. After the culture supernatant was fully reacted with the kit, the OD of each well was determined by a microplate reader set to 450 nm. Then, a standard curve was created according to the standard sample concentration, and the concentration of the sample to be tested was read

from the standard curve. Experiments were performed at least three times for each sample.

Statistical analysis

The statistical software Prism 7 (GraphPad Software) was used for data analyses. Statistical significance was determined by a Student *t* test. Multiple means were compared by one-way ANOVA. Error bars in the figures indicate the SEM. Statistical significance was set at $p < 0.05$. Statistically significant results are expressed as follows: $*p < 0.05$, $**p < 0.01$, $***p < 0.001$.

Data availability

The MeRIP-seq data generated in this study have been deposited in Gene Expression Omnibus under accession number GSE242071 (https://www.ncbi.nlm.nih.gov/geo/query/acc.cgi?acc=GSE242071). The data that support the findings of this study are available from the corresponding author upon reasonable request.

Results

The expression levels of m6A and METTL14 in cervical cancer

Initially, we performed m6A MeRIP-seq in which we compared the m6A profile and motifs of cervical cancer tissues with those of paracancerous tissue. Areas with m6A modifications included the 3′ untranslated region (UTR), coding sequence (CDS), 5′UTR, and other regions. Remarkably, the m6A peaks were mainly located in the 3′UTR area and the end of the CDS (Fig. 1A). Fig. 1B indicates that compared with paracancerous tissue, the m6A peaks distributed in the area surrounding the stop codon and 3′UTR increased in cervical cancer tissue. In addition, the distribution level of the m6A peak on the mRNA of cervical cancer tissues was higher than that in paracarinoma tissues (Fig. 1C). By using HOMER software, we performed motif analysis on peaks: a typical motif with m6A modification is GGAC. The results showed the GGAC motif sequence was mainly distributed in cervical cancer tissues (Fig. 1D). An m6A RNA methylation quantification kit was used to detect m6A RNA methylation status using total RNA. The results showed an increase in m6A levels in total RNA isolated from cervical cancer tissues (Fig. 1E). In conclusion, MeRIP-seq revealed hundreds of m6A peaks in cervical cancer tissues, which show that m6A was upregulated. Fig. 1F and 1G suggested that the genes associated with differential m6A modifications are mainly related to tumor pathways. We investigated the relationship between the expression of m6A methylation-related genes and survival rate (Supplemental Fig. 1A) and found that only METTL14 expression significantly affected the overall survival rate. Survival analysis by the Spearman rank correlation coefficient (GEPIA, http://gepia.cancer-pku.cn/) showed that higher levels of METTL14 expression indicated poor overall survival in cervical cancer (Fig. 1H). Conversely, genes encoding other m6A methylation-related enzymes had no significant impact on the prognosis (Supplemental Fig. 1A). This result indicates that METTL14 is an important gene that regulates m6A methylation, and it may play an important role in the genesis and development of tumors.

Next, we performed immunohistochemistry and Western blotting, which indicated that the protein expression of METTL14 was upregulated in cervical cancer tissues ($n = 10$) compared with that in paracarcinoma tissues ($n = 10$) (Fig. 1I, 1K). Statistical results are shown in Fig. 1J and 1L. Similarly, using qPCR, we confirmed an increase of the RNA expression of METTL14 in cervical cancer tissues (Fig. 1M).

METTL14 has a role in tumor cell survival and migration

We aimed to validate the role of METTL14 in cervical cancer cell lines by upregulating or downregulating its expression in CaSki cells using shRNA (Supplemental Fig. 1B). The statistical results are shown in Figs. 4G and 6J. The sequences of shRNA and sh-NC are shown in the supplemental material. The results of the Cell Counting Kit-8 assay and EdU assay showed that the cell proliferation ability was significantly decreased after METTL14 downregulation and increased after upregulation (Supplemental Fig. 1C–E).

When DNA damage, whether endogenous or exogenous, forms double-stranded breaks, it is always followed by phosphorylation of histone γ-H2AX (33). The detection of γ-H2AX via immunofluorescence allows for the assessment of DNA damage and repair and their related proteins. Supplemental Fig. 1F and 1G show representative immunofluorescence images of γ-H2AX in METTL14 knockdown cells, METTL14 overexpression cells, and the NC group. More DNA damage was present in the METTL14 shRNA group than in the NC group, whereas less damage was present in the METTL14 overexpression group.

Cell migration assays revealed that fewer cells successfully penetrated the membrane in the METTL14 shRNA group than those in the sh-NC group. Conversely, cell migration was enhanced in the METTL14 overexpression group (Supplemental Fig. 1H, 1I). This indicates that METTL14 plays a crucial role in regulating tumor cell activity.

The number of M2 macrophages expressing PD-1 increases in cervical cancer

We further investigated macrophage infiltration in tumor lesions and paracarcinoma tissues from patients with cervical cancer. Notably, the immunofluorescence analysis revealed a higher percentage of PD-1$^+$ M2 macrophages (PD-1$^+$CD206$^+$) in the tumor lesions ($n = 10$) than in the paracarcinoma tissues ($n = 10$) (Fig. 2A, 2B). The appearance confirmed that the infiltration of macrophages in cervical cancer tended to be of the M2 type, while the expression of PD-1 was higher.

METTL14 promotes PD-1 expression and inhibits phagocytotic function in M2 macrophages

Macrophages derived from THP-1 cells were collected after being cocultured with METTL14 shRNA CaSki cells or sh-NC CaSki cells (Supplemental Fig. 2B). The results of qPCR indicated that macrophages cocultured with METTL14 shRNA cells had lower levels of M2-related cytokine expression (Fig. 2C). Consistent results were noted in the ELISA determination of cytokine production by macrophages. The concentration of cytokines secreted by M2 macrophages such as IL-10 and TGF-β in culture supernatant increased after cocultured with METTL14 shRNA cells (Fig. 2D). Flow cytometry showed that there were fewer M2 macrophages (CD206$^+$CD163$^+$) in the group involving macrophages cocultured with METTL14 shRNA CaSki cells than in the control group (Fig. 2E, 2F). In addition, the PD-1 expression in M2 macrophages increased after coculture with METTL14 shRNA CaSki cells (Fig. 2G, 2H). Immunofluorescence results indicated the same trend (Fig. 2I, 2J).

Flow cytometry and immunofluorescence were used to determine macrophage phagocytosis. The double-positive cells in the cell mixture represent macrophages that successfully devour tumor cells. The flow diagram of the phagocytosis experiment is shown in the Supplemental Fig. 3A. As shown in Fig. 2K and 2L, the METTL14 shRNA group exhibited higher levels of phagocytosis than the control group. The cell mixtures were imaged via microscopy (Fig. 2M). The results demonstrated that more THP-1–derived macrophages phagocytosed shMETTL14 cancer cells than NC cells.

To further demonstrate the impact of PD-1 expression on the phagocytic function of macrophages, anti–PD-1 Ab was added to THP-1–derived macrophages to block the activity of PD-1. The results demonstrated that more THP-1–derived macrophages phagocytosed cancer cells after using anti–PD-1 Ab (Supplemental Fig. 2C).

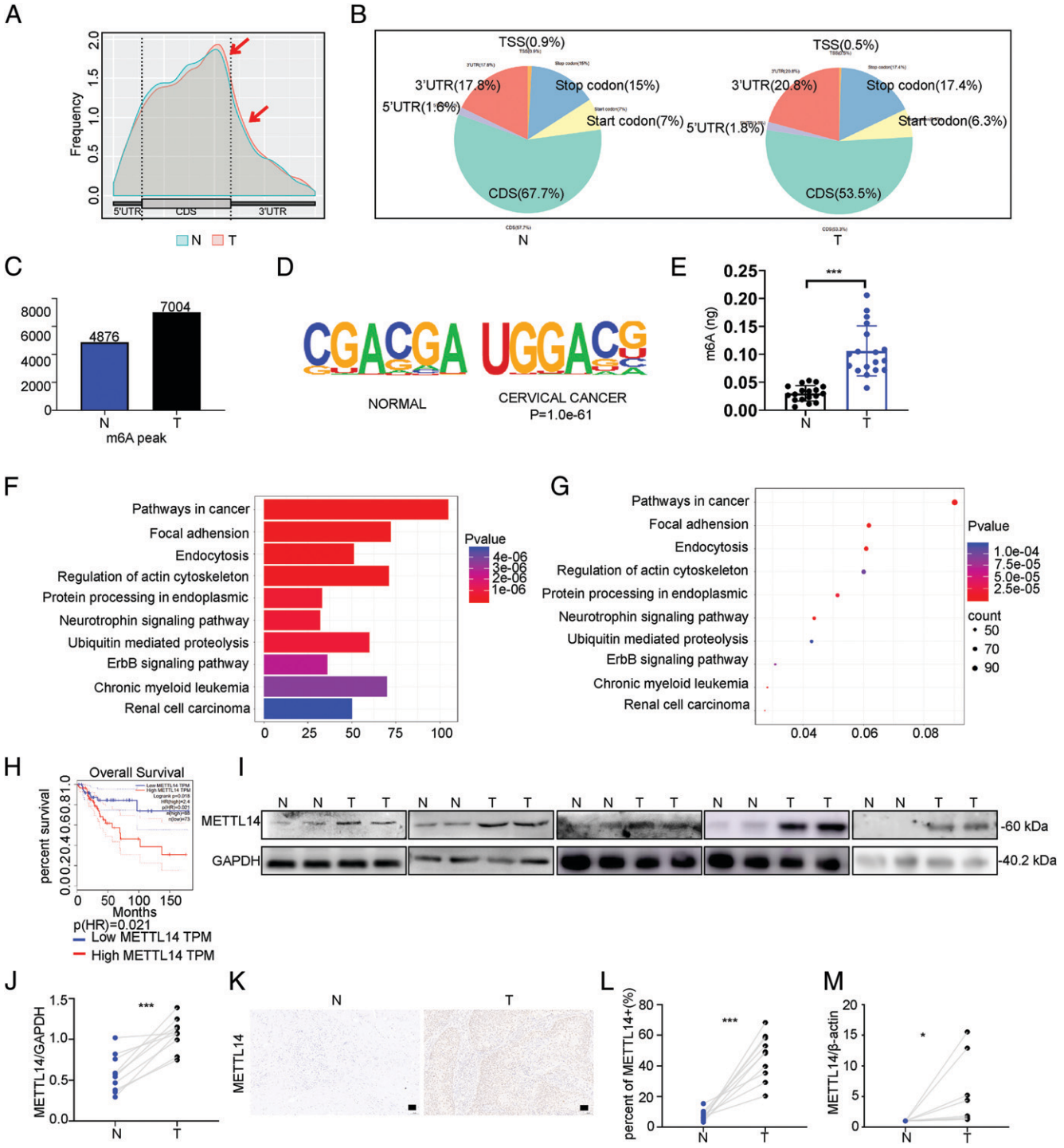

FIGURE 1. m6A methylation and METTL14 expression increase in the cervical cancer tissues. (**A** and **B**) MeRIP-seq assays reveal that the m6A peaks were mainly located in the surrounding area of the stop codon, 3′UTR, and the end of the CDS. (**C**) Number of m6A peaks. (**D**) Motif sequences in cervical carcinoma and adjacent tissues. (**E**) Level of m6A of RNA. (**F** and **G**) KEGG analysis shows that the difference between cervical cancer and paracancerous tissue tissues is mainly reflected in tumor-related pathways. (**H**) Survival analysis by Spearman rank correlation coefficient (GEPIA, http://gepia.cancer-pku.cn/) shows that a higher METTL14 expression indicated a poor survival rate for cervical cancer. (**I** and **J**) Protein level of METTL14 in cervical cancer ($n = 10$) and paracancerous tissues ($n = 10$). GAPDH served as a loading control. (**K** and **L**) Representative micrographs of METTL14 immunostaining in cervical cancer and paracancerous tissues. Quantitative analysis of the percentage of positive cells for METTL14 immunostaining in tumor lesions or control tissues. Scale bars, 50 μm. (**M**) mRNA level of METTL14 in cervical cancer ($n = 10$) and paracancerous tissues ($n = 10$). Results represent the mean ± SD. *$p < 0.05$, ***$p < 0.001$. N, cervical cancer; T, paracancerous tissue.

METTL14 promotes M2 macrophages expressing PD-1 in vivo

TC-1 cells transfected with METLL14 shRNA or sh-NC were injected s.c. into C57BL/6J mice to establish an animal model of cervical cancer (Fig. 2N). This animal experiment was used to observe the effect of METTL14 on the phenotype and infiltration of macrophages in mice with a normal immune state. The results showed that the s.c. tumor volume in the METTL14 shRNA group ($n = 6$) increased to a lesser extent than that in the control group

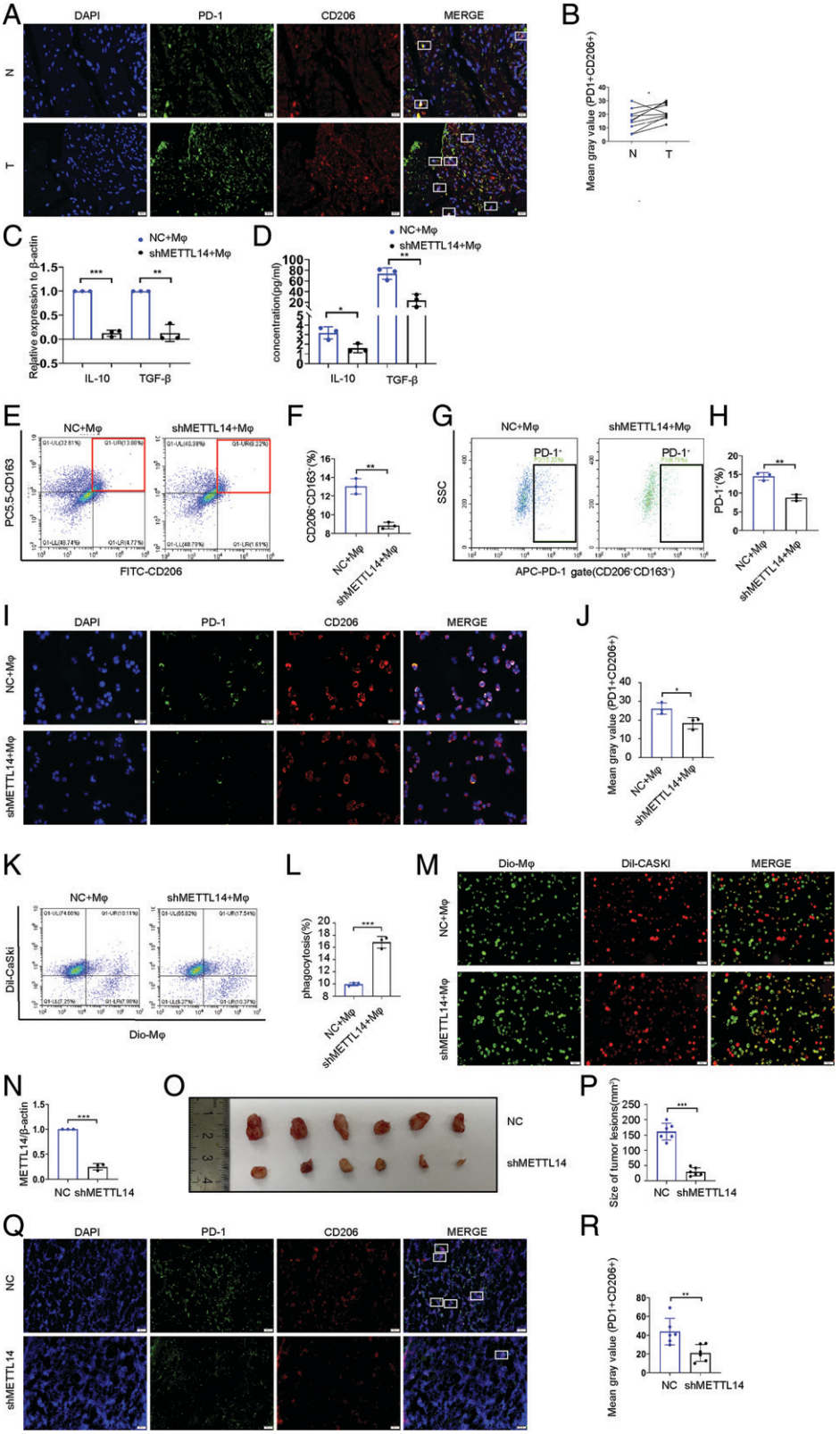

FIGURE 2. Abnormal aggregation of PD-1$^+$ M2 macrophages in cervical cancer and the effect of METTL14 on PD-1$^+$ M2 macrophages. (**A**) Tissue immunofluorescence shows the aggregation of PD-1$^+$ M2 macrophages. Red fluorescence represents CD206 (a marker for M2 macrophages); green fluorescence represents PD-1. Cells within a white box are cells that collectively express CD206 and PD-1, that is, PD-1$^+$ M2 macrophages. Scale bars, 20 μm. (**B**) Mean gray density at both red and green fluorescence labeled simultaneously. (**C**) mRNA level of IL-10 and TGF-β in THP-1–derived M2 macrophages after coculture with CaSki cells with METTL14 shRNA or NC. (**D**) Concentration of IL-10 and TGF-β in cell supernatant. (**E** and **F**) Representative and quantitative flow cytometry results for CD206 and CD163 (M2 marker) in THP-1–derived M2 macrophages after coculture with CaSki cells with METTL14 shRNA or NC. (**G** and **H**) Positive rate of PD-1 in the CD206$^+$CD163$^+$ cell population. (**I**) Immunofluorescence indicates the PD-1 expression of THP-1–derived M2 macrophages after coculture with CaSki cells with METTL14 shRNA or NC. Red fluorescence represents CD206, and green fluorescence represents PD-1. Scale bars, 50 μm. (**J**) Mean gray density at both red and green fluorescence labeled simultaneously. (**K** and **L**) *(Figure legend continues)*

($n = 6$) (Fig. 2O, 2P). The immunofluorescence analysis revealed a lower percentage of PD-1$^+$ M2 macrophages (PD-1$^+$CD206$^+$) in the METTL14 shRNA group ($n = 6$) than in the control group ($n = 6$) (Fig. 2Q, 2R). The appearance confirmed that the infiltration of macrophages in the METTL14 shRNA group strayed from the M2 type, whereas the expression of PD-1 was lower.

Lactic acid from tumor cells promotes PD-1 expression and inhibits macrophage function in M2 macrophages

We examined the metabolites in tumor cell supernatants that may affect the function and polarization of macrophages. We found significant changes in lactic acid levels in CaSki cell supernatants with reduced METTL14 expression, whereas the fatty acid and NO content did not change significantly (Fig. 3A).

The mechanism by which lactic acid affects macrophages is mainly through the activation of GPR81 on the surface of macrophages (34–37). Therefore, on macrophages, we used GPR81 siRNA to inhibit the expression of GPR81 on the surface of macrophages, thereby blocking the effect of lactic acid on macrophages. qPCR experiments showed that siGPR81 expression in macrophages was successfully knocked down (Fig. 3B). In this experiment, THP-1–derived M2 macrophages transfected with siGPR81 or si-NC were coculture with CaSki cells (Supplemental Fig. 2C). The levels of M2-related cytokines (IL-10, TGF-β) in macrophages were reduced in THP-1–derived M2 macrophages transfected with GPR81 siRNA (Fig. 3C). The detection of secreted protein levels of IL-10 and TGF-β using ELISA assays indicated the same trend (Fig. 3D). Simultaneously, flow cytometry and immunofluorescence analysis showed that there were fewer M2 macrophages in the GPR81-downregulated group than in the control group (Fig. 3E, 3F). At the same time, the number of PD-1$^+$ cells decreased in the group of M2 macrophages (Fig. 3G–J). We used macrophage phagocytosis as a marker to assess macrophage functions. The flow diagram of the phagocytosis experiment is shown in Supplemental Fig. 2A. Flow cytometry results show that the number of macrophages that successfully phagocytosed tumor cells increased significantly in the siGPR81 macrophage group (Fig. 3K, 3L). Immunofluorescence analysis showed the same trend (Fig. 3M).

Our results suggest that tumor cell–derived lactic acid acts on macrophages, leading to changes in PD-1 expression and phagocytic function of M2 macrophages.

Glycolysis is upregulated in cervical cancer lesions

We measured the glycolysis levels in cervical cancer because lactic acid is mainly produced by glycolysis. To do so, we detected the expression of PKM2 and HK2, which are enzymes that play a crucial role in glycolysis. The results of immunohistochemistry indicated that the protein expression levels of PKM2 and HK2 were upregulated in the cervical cancer lesions compared with those in the paracancerous lesions (Fig. 4A, 4B). Similarly, qPCR also showed that the mRNA levels of PKM2 and HK2 in the cervical cancer lesions ($n = 10$) were significantly higher than those the paracancerous tissue ($n = 10$) (Fig. 4C). Western blotting revealed increased protein expressions of PKM2 and HK2 in cervical cancer tissue (Fig. 4D, 4E). These results suggest that cervical cancer tissues are associated with increased glycolysis levels.

METTL14 knockdown decreases glycolysis levels and promotes apoptosis

Changes in the protein levels of PKM2 and HK2 were observed in METTL14 shRNA cells (Fig. 4F, 4G). The results of targeted metabolomics sequencing showed that the levels of metabolites related to glucose metabolism, including lactic acid, changed significantly after a decrease in METTL14 expression (Fig. 4H). The thermogram of metabolite content and Z score results of metabolomics are shown in Supplemental Fig. 2A and 2B. ECAR and OCR assays showed that the low expression of METTL14 markedly suppressed glycolytic capacity (Fig. 4I). Oxidative phosphorylation (OXPHOS) is an active metabolic pathway in many cancers, so it is necessary to eliminate the influence of OXPHOS. Flow cytometry results showed that although the inhibition of OXPHOS using rotenone and antimycin A could alter macrophage polarization (Supplemental Fig. 2D), the impact on PD-1 expression was minimal (Supplemental Fig. 2E). In addition, this change is not sufficient to affect the phagocytic function of macrophages (Supplemental Fig. 2F).

The s.c. tumor-bearing model of cervical cancer was established in BALB/c nude mouse using CaSki cells, so that the effect of METTL14 on the proliferation and glycolysis levels of cervical cancer could be further verified in vivo. The results showed that the s.c. tumor volume in the METTL14 shRNA group increased to a lesser extent than that in the control group (Fig. 4J, 4K). In addition, immunohistochemistry results suggested that there was less expression of PKM2 and HK2 in METTL14 shRNA tumor lesions than that in the control group (Fig. 4L, 4M). Furthermore, a TUNEL assay was used to detect the level of apoptosis in mouse s.c. tumors. The results showed a higher level of apoptosis in the s.c. tumor of the METTL14 shRNA group (Fig. 4N, 4O).

Overall, our findings revealed that METTL14 promoted glycolysis in CaSki cells.

Lactic acid produced by tumor glycolysis and mediated by METT14 affects macrophage phenotype and function

The effect of METTL14 on macrophage polarization and PD-1 expression may be mediated by regulating the lactic acid produced by glycolysis. To reduce the concentration of lactic acid, the glycolysis inhibitor 2-DG was used to create a glycolysis inhibition model in CaSki cervical cancer cells. To prove that the effect of METTL14 on macrophages is dependent on the lactic acid produced by tumor glycolysis, CaSki cells overexpressing METTL14 were treated with 2-DG (Supplemental Fig. 2D). In this cell model, the increased glycolytic level caused by overexpression of METTL14 can be inhibited by 2-DG. Also, the Western blot results suggested that overexpressed METTL14 does not affect the expression of METTL3 on its hetero-complex (Supplemental Fig. 2G, 2H). As shown in Supplemental Fig. 3D, cells were divided into three groups: macrophages cocultured with control CaSki cells, macrophages cocultured with CaSki cells overexpressing METTL14, and macrophages cocultured with glycolysis-inhibited CaSki cells overexpressing METTL14. The qPCR

Phagocytosis is quantified as the percentage of double fluorophore-positive macrophages confirmed by flow cytometry analysis. (**M**) Representative images are shown for CaSki cells stained with Dil, transfected with shMETTL14 or NC, and cultured with THP-1 cells stained with Dio. Scale bars, 50 μm. (**N**) qPCR analysis of METTL14 mRNA expression in TC-1 transfected with METLL14 shRNA or sh-NC. (**O**) TC-1 cells, with METTL14 shRNA or sh-NC, were s.c. inoculated into C57BL/6J mice. Each group consisted of six mice. (**P**) Tumor size. (**Q**) Tissue immunofluorescence indicates the aggregation of PD-1$^+$ M2 macrophages. Red fluorescence represents CD206, and green fluorescence represents PD-1. Cells within a white box are cells that collectively express CD206 and PD-1, that is, PD-1$^+$ M2 macrophages. Scale bars, 50 μm. (**R**) Mean gray density at both red and green fluorescence labeled simultaneously. *$p < 0.05$, **$p < 0.01$, ***$p < 0.001$. NC, negative control.

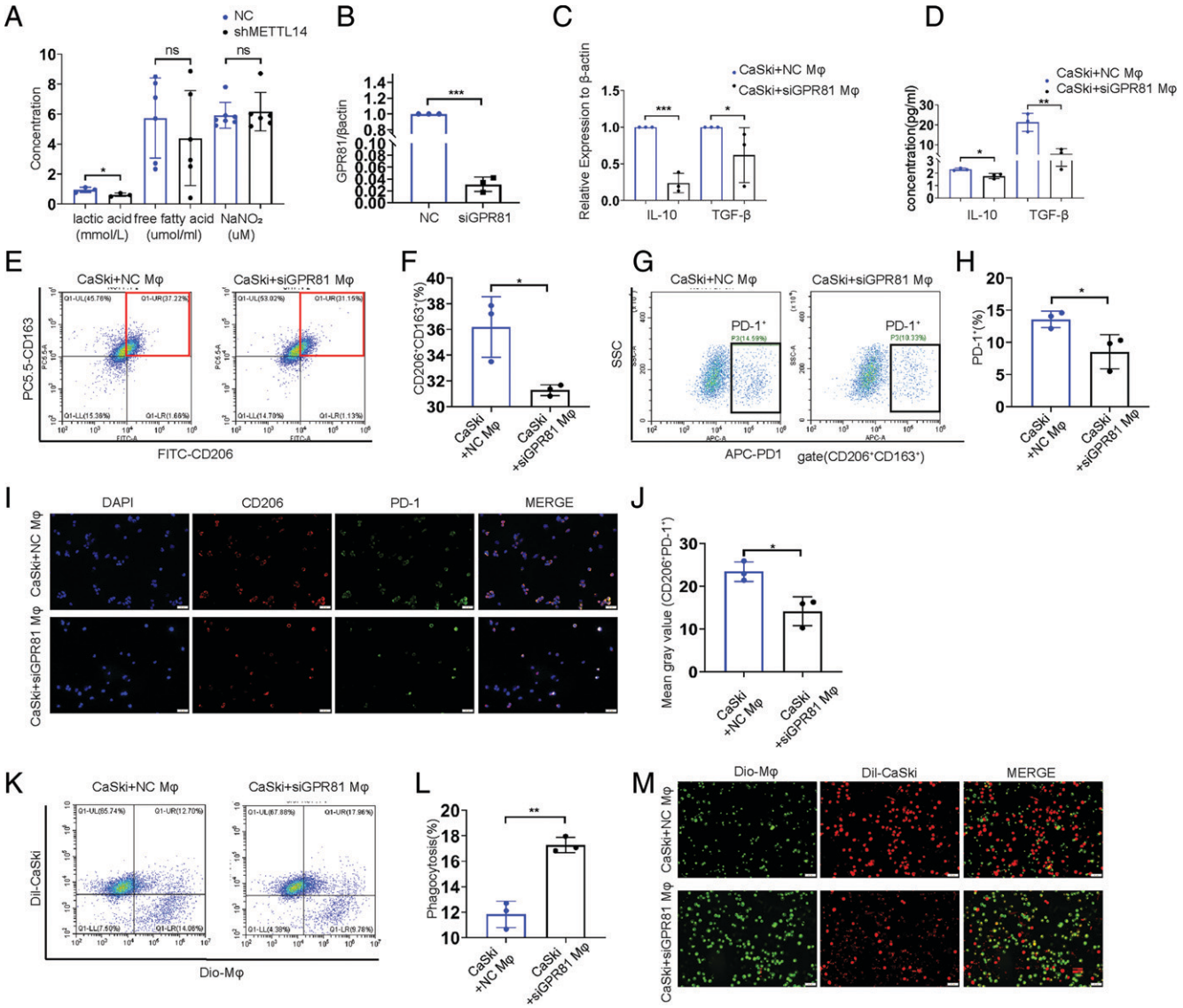

FIGURE 3. Lactate acid from tumors leads to changes in M2 macrophage function and PD-1 expression. (**A**) Lactic acid, fatty acid, and NO concentrations in the CaSki cell supernatant. (**B**) qPCR analysis of GPR81 mRNA expression in NC macrophages cocultured with CaSki cells and GPR81 siRNA macrophages cocultured with CaSki cells. β-Actin served as a loading control. (**C**) IL-10 and TGF-β mRNA levels in NC macrophages cocultured with CaSki cells and GPR81 siRNA macrophages cocultured with CaSki cells. β-Actin served as a loading control. (**D**) Concentration of IL-10 and TGF-β in cell supernatant. (**E** and **F**) Representative and quantitative flow cytometry results for CD206 and CD163 (M2 marker) in NC macrophages cocultured with CaSki cells and GPR81 siRNA macrophages cocultured with CaSki cells. (**G** and **H**) Positive rate of PD-1 in the $CD206^+CD163^+$ cell population. (**I** and **J**) Immunofluorescence analysis shows the expression of PD-1 and CD206 in NC macrophages cocultured with CaSki cells and GPR81 siRNA macrophages cocultured with CaSki cells. Scale bars, 50 μm. (**K** and **L**) Phagocytosis is quantified as the percentage of double fluorophore-positive THP-1–derived macrophages and is confirmed by flow cytometry analysis. (**M**) Representative images show CaSki cells stained with Dil and cultured with THP-1–derived macrophages stained with Dio that were transfected with siRNA or NC. Scale bars, 50 μm. $^*p < 0.05$, $^{**}p < 0.01$, $^{***}p < 0.001$.

(Fig. 5A) and ELISA (Fig. 5B) results indicate that the upregulation of M2-related cytokines in the METTL14 overexpression group was significantly reversed after the 2-DG treatment. In addition, flow cytometry results showed that although METTL14 overexpression simultaneously increased the total number of M2 macrophages and the number of $PD\text{-}1^+$ M2 macrophages, inhibition of tumor glycolysis via 2-DG reduced the M2 macrophage polarization and PD-1 expression (Fig. 5C–F). Immunofluorescence analysis showed an increase in M2 macrophages expressing PD-1 ($PD\text{-}1^+$ $CD206^+$) in the METTL14 overexpression group (Fig. 5G, 5H). However, compared with the group in which macrophages were cocultured with METTL14 overexpression CaSki cells, decreased expression of CD206 and PD-1 in macrophages was observed after coculturing with METTL14 overexpression CaSki cells treated with 2-DG (Fig. 5G, 5H). In phagocytosis experiments, we found that tumor cells overexpressing METTL14 were less easily recognized and phagocytosed by macrophages than those in the control group. However, this phenomenon of immune evasion disappeared with glycolysis inhibition (Fig. 5I, 5J). The cell mixtures were imaged via microscopy (Fig. 5K). In addition, as shown in Supplemental Fig. 2I and 2J, macrophages moved away from the M2 type when they were cocultured with CaSki cells added with 2-DG alone. At the same time, the number of $PD\text{-}1^+$ M2 macrophages decreased (Supplemental Fig. 2K). However, when excessive expression of METTL14 and 2-DG simultaneously acted on CaSki cells, the cocultured macrophages showed an increasing trend in the polarization

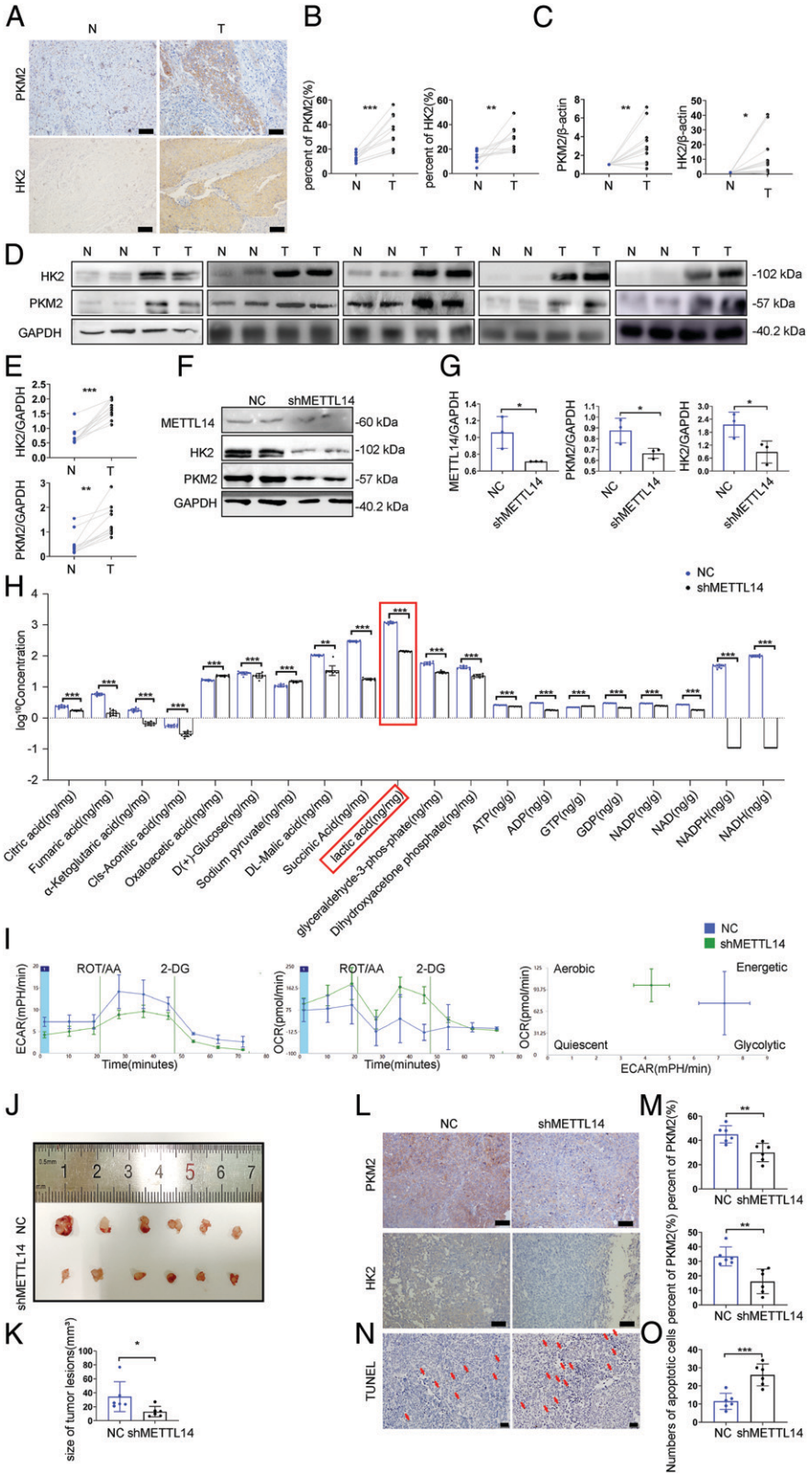

FIGURE 4. Glycolysis is increased in cervical cancer tissues, but METTL14 downregulation inhibits glycolysis in CaSki cell lines in vivo and in vitro. (**A** and **B**) Representative micrographs of PKM2 and HK2 immunostaining in cervical cancer ($n = 10$) and paracancerous tissues ($n = 10$). Quantitative analysis of the percentage of cells positive for PKM2 and HK2 immunostaining in tumor lesions and paracancerous tissues. Scale bars, 50 μm. (**C**) PKM2 and HK2 mRNA levels in cervical cancer ($n = 10$) and paracancerous tissues ($n = 10$). (**D** and **E**) Protein levels of PKM2 and HK2 in cervical cancer ($n = 10$) and paracancerous tissues ($n = 10$). GAPDH serves as the loading control. (**F** and **G**) Protein levels of HK2 and PKM2 in CaSki cell lines in which METTL14 was downregulated by shRNA. GAPDH serves as the loading control. (**H**) Quantitative analysis of the metabolites related to glucose metabolism. The quantitative result of lactic acid is marked by a red frame. (**I**) Cellular ECAR and OCR were measured by Seahorse. (**J**) CaSki cells, with or without METTL14 shRNA, were s.c. inoculated into nude mice. Each group consisted of six mice. (**K**) Tumor size. (**L** and **M**) Representative micrographs of PKM2 and HK2 immunostaining in the shMETTL14 and control groups and quantitative analysis of the percentage of positive cells. Scale bars, 50 μm. (**N** and **O**) Representative micrographs of TUNEL staining for apoptosis in shMETTL14 and control groups. A TUNEL-positive apoptotic cell is indicated by a red arrowhead, and the apoptotic nuclei that show DNA fragmentation appear dark brown. Scale bars, 50 μm. $^{*}p < 0.05$, $^{**}p < 0.01$, $^{***}p < 0.001$. N, cervical cancer; T, paracancerous tissue.

level or PD-1 expression (Supplemental Fig. 2I–K). Even so, this group of macrophages showed no significant difference compared with the control group. Collectively, these results suggest tumor glycolysis plays a role in the relationship between METTL14 and expression of PD-1 in M2 macrophages.

AMPKα plays a role in the regulation of glycolysis by METTL14

NAD is the main electron carrier coenzyme for the oxidation of all energy substrates, including glucose, fatty acids, and ketones. The results of targeted metabolomics sequencing showed a decrease in low expression of NAD^{+} expression in the METTL14 shRNA cells.

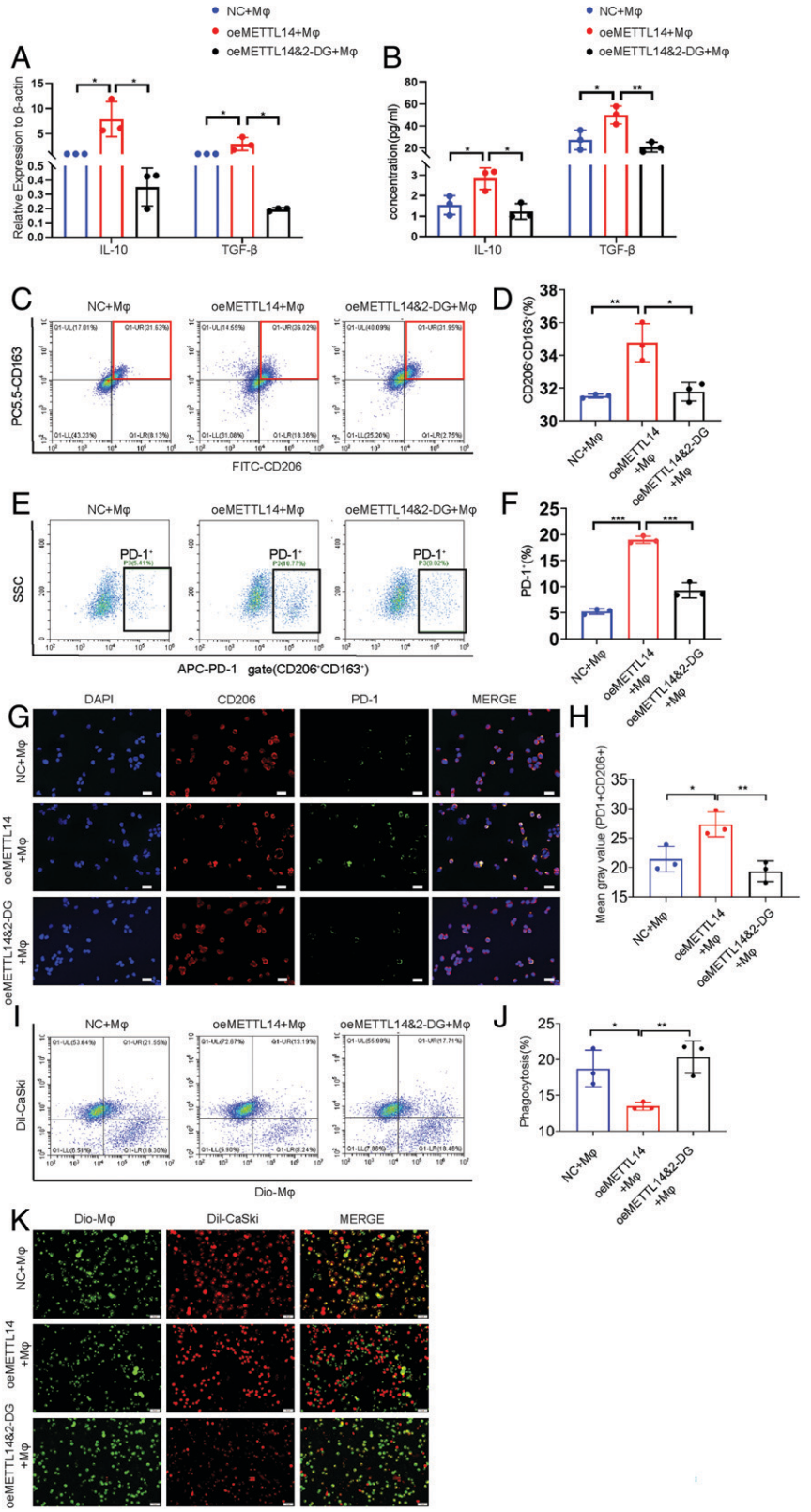

FIGURE 5. METTL14 regulates the glycolysis of tumor cells to produce lactic acid, thereby affecting the phenotype and function of macrophages. Cells were divided into the following three groups: macrophages cocultured with CaSki cells, macrophages cocultured with CaSki cells overexpressing METTL14, and macrophages cocultured with glycolysis-inhibited CaSki cells overexpressing METTL14. (**A**) IL-10 and TGF-β mRNA levels in each group. (**B**) Concentration of IL-10 and TGF-β in cell supernatant. (**C** and **D**) Representative and quantitative flow cytometry results of CD206 and CD163 (M2 marker) in each group. (**E** and **F**) Positive rate of PD-1 in the $CD206^{+}CD163^{+}$ cell population. (**G** and **H**) Immunofluorescence analysis indicates PD-1 expression in M2 macrophages in each group. Scale bars, 50 μm. (**I** and **J**) Phagocytosis is quantified as the percentage of double fluorophore-positive THP-1–derived macrophages, which is confirmed by flow cytometry analysis. (**K**) Representative images showing CaSki cells stained with Dil and THP-1 cells stained with Dio. Scale bars, 50 μm. $^{*}p < 0.05$, $^{**}p < 0.01$, $^{***}p < 0.001$.

The AMPK signaling pathway plays an important role in regulating cellular NAD^{+} levels. Therefore, the AMPK signaling pathway may affect the METTL14-mediated regulation of glycolysis (Fig. 6A). The regulation of AMPK on cellular metabolism is mainly achieved through function of the α subunit.

The SRAMP prediction server (http://www.cuilab.cn/sramp) was used to predict the sequences and structural features around m6A sites. The prediction result indicated that there are multiple m6A modification sites on AMPK, and this study selected the sites with the highest reliability for verification (AUUCU UGCAC AAUAA

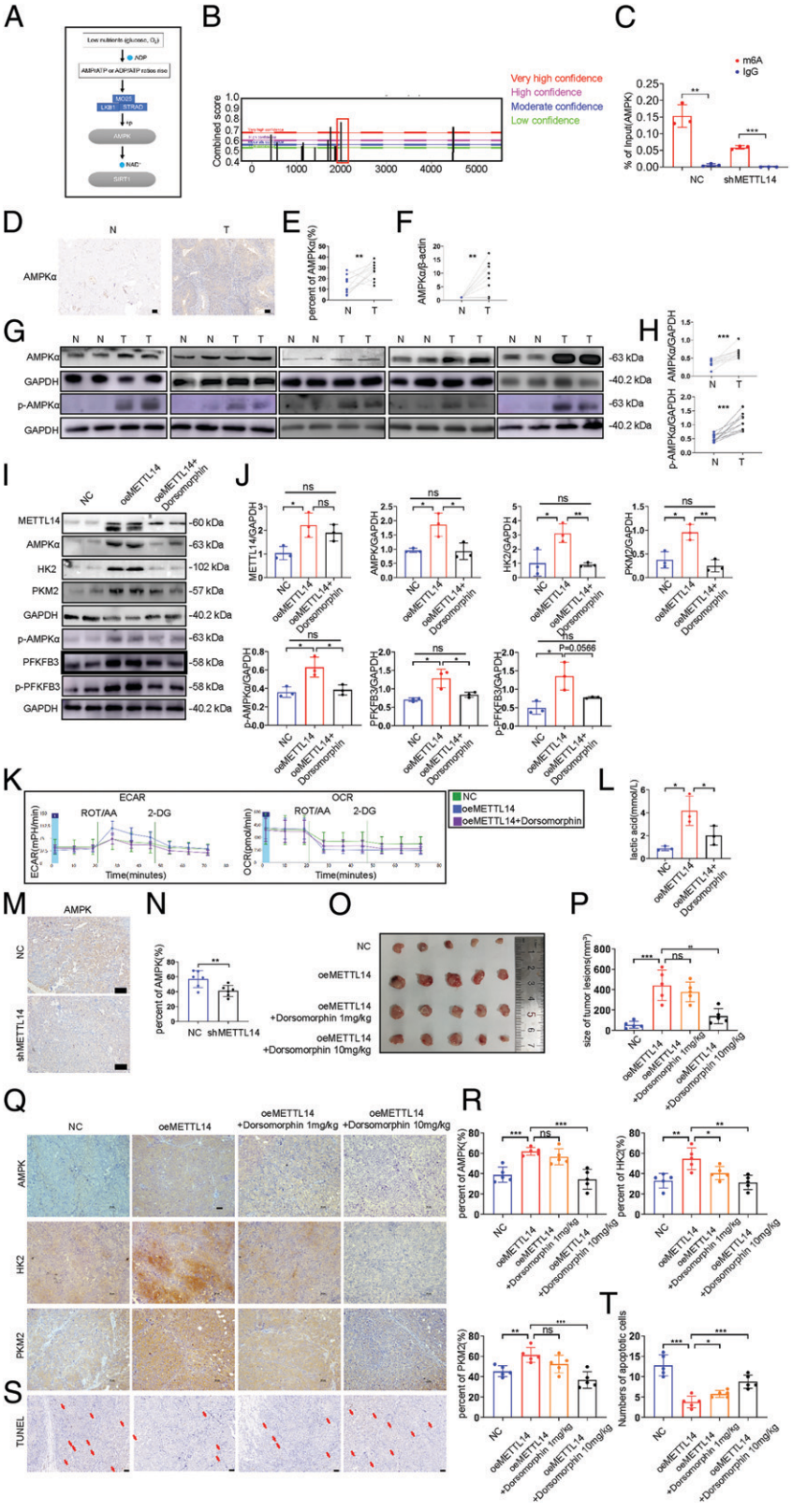

FIGURE 6. AMPKα regulates glycolysis via METTL14, and cervical cancer tissues exhibit aberrant AMPK expression. (**A**) KEGG pathway analysis of AMPK; blue points indicate decreased expression when METTL14 was downregulated by shRNA. (**B**) Sequences and structural features around m6A sites on AMPK were predicted by SRAMP server (http://www.cuilab.cn/sramp). The segment sequence with the highest confidence level is marked with a red frame. (**C**) MeRIP-qPCR indicated the AMPK mRNA enrichment precipitated by m6A Ab. (**D** and **E**) Immunochemistry analysis of AMPKα expression in cervical cancer ($n = 10$) and control tissues ($n = 10$). Scale bars, 50 μm. (**F**) qPCR analysis of AMPK expression in cervical cancer ($n = 10$) and control tissues ($n = 10$). (**G** and **H**) Western blot analysis of AMPKα and p-AMPKα expression in cervical cancer and control tissues. GAPDH is the sample loading control. (**I** and **J**) Using a Western blot, the protein levels of AMPKα, p-AMPKα, and its downstream molecule were detected after METTL14 was upregulated. Results of the Western blot indicate that AMPKα was successfully inhibited by dorsomorphin, and the protein expression of PKM2 and HK2 changed correspondingly. (**K**) Cellular ECAR and OCR were measured by Seahorse. (**L**) Lactate production. (**M** and **N**) Representative micrographs of the subcutaneous tumor. AMPK immunostaining is shown of the shMETTL14 and sh-NC groups as well as the quantitative analysis of positive cells (%). Scale bars, 50 μm. (**O** and **P**) Animals were divided into the following four groups: control group (NC), METTL14 overexpression group (oeMETTL14), METTL14 overexpression and injection of AMPK inhibitor group (oeMETTL14+dorsomophin at 1 or 10 mg/kg). Each group contained five mice. (**Q** and **R**) Representative micrographs of AMPK, HK2, and AMPK immunostaining in each group. Scale bars, 20 μm. (**S** and **T**) Representative micrographs of TUNEL staining for apoptosis in each group. Scale bars, 50 μm. $*p < 0.05$, $**p < 0.01$, $***p < 0.001$. ns, not significant.

ACAGA AAACU UUGCU UAUUU CUUUU GCAGC) (Fig. 6B). MeRIP-qPCR indicated that m6A modification exists on AMPK, whereas METTL14 knockdown decreased the AMPK mRNA level precipitated by m6A Ab (Fig. 6C).

The expression of AMPK was identified in patients with cervical cancer using immunohistochemistry analysis. AMPKα immunoreactivity was significantly higher in the tumor tissues than in the paracarinoma tissues (Fig. 6D, 6E). qPCR revealed an increase in AMPK mRNA levels in cervical cancer tissues compared with those in the adjacent tissues (Fig. 6F). To verify this, Western blotting was performed, which demonstrated an increase in AMPKα protein levels in cervical cancer tissues (Fig. 6G, 6H). At the same time, the level of AMPK phosphorylation

also increased (Fig. 6G, 6H). Altogether, these findings identified the abnormal expression of AMPKα in cervical cancer and this phenomenon is likely to be in contact with METTL14 and glycolysis.

We overexpressed METTL14 in functional experiments to further investigate the relationship between METTL14, AMPK, and glycolysis. After the expression of METTLL14 increased, the elevated protein levels of AMPKα and p-AMPKα were detected. Meanwhile, the overexpression of METTL14 also affected the downstream molecule PFKFB3 of AMPK and its phosphorylation. Correspondingly, the key enzymes of glycolysis (HK2, PKM2) also increased (Fig. 6I, 6J). ECAR and OCR assays showed that METTL14 markedly promoted glycolytic capacity (Fig. 6K). Energy metabolism analysis indicated that METTL14 overexpression promoted lactate production (Fig. 6L).

Dorsomorphin (compound C) is a selective and ATP-competitive AMPK inhibitor. In the CaSki cell line, dorsomorphin successfully inhibited AMPKα and p-AMPKα expression, resulting in the impairment of glycolytic function (Supplemental Fig. 2L). At the same time, in the CaSki cells with high expression of METTL14, dorsomorphin treatment was also associated with a decrease in PKM2 and HK2 expression, which had initially increased because of METTL14 overexpression (Fig. 6I, 6J). Simultaneously, lactate production and ECAR decreased (Fig. 6J, 6K) whereas OCR increased (Fig. 6K). Interestingly, when dorsomorphin acted on the CaSki cells that overexpressed METTL14, the glycolysis level of the tumor cells was lower than that of the METTL14 overexpression group (Fig. 6I, 6J) and higher than that of the dorsomorphin alone group (Supplemental Fig. 2L). Collectively, these results suggest that AMPK participates in glycolysis downregulation.

METTL14 affects glycolysis mainly via AMPK in vivo

AMPKα expression in the s.c. tumors in Fig. 4J was lower in the METTL14 shRNA group than it was in the control group (Fig. 6M, 6N). CaSki cells were used to establish a mouse model of cervical cancer. In addition, this experiment verified the role of the AMPKα pathway in the process of glycolysis, which is regulated by METTL14. Compared with the control group, the METTL14 overexpression group exhibited a significant increase in tumor volume. When a sufficient AMPK inhibitor (dorsomorphin) was injected i.p. into mice overexpressing METTL14, we observed that the tumor volume (Fig. 6O, 6P) and AMPKα expression (Fig. 6Q, 6R) were successfully inhibited by dorsomorphin. Immunohistochemical results suggested that the expression levels of PKM2 and HK2 were downregulated in mouse tumors after dorsomorphin injection compared with that in the group overexpressing METTL14 (Fig. 6Q, 6R). Additionally, TUNEL staining showed lower apoptosis levels in the s.c. tumors in the METTL14 overexpression group than in the control group. However, after AMPK expression was inhibited, the rate of apoptosis in the tumor increased (Fig. 6Q, 6R). Animal experiments confirmed our previous results indicating that METTL14 can promote tumor growth by promoting tumor glycolysis through the AMPK pathway.

Discussion

Recent developments in the biology of cervical cancer revealed that epigenetic alterations, including DNA methylation, histone modification, and long noncoding RNA regulation, are common in cervical carcinogenesis and the immune response (38). However, the potential role of RNA m6A modification patterns are poorly defined in cervical cancer and macrophage function. Previous studies have demonstrated that m6A RNA methylation regulators are associated with cancer invasion and patient survival (39). Although m6A RNA methylation could act as an oncogene or tumor suppressor gene to contribute to the occurrence and progression of various cancers (40–42), its research in cervical cancer is still lacking. In this study, we have demonstrated that the levels of m6A methylation and methyltransferase METTL14 expression are highly increased in cervical cancer tissues compared with paracancerous tissues. In addition, with the knockdown of METTL14 in vitro, cell apoptosis rates decreased whereas proliferation and migration levels were enhanced. Animal studies showed similar trends. These data in our study indicate that METTL14 can act as an oncogenic element in cervical cancer tumorigenesis. The abnormal METTL14 expression is related to biological function of tumor cells.

PD-1 was initially discovered to be a molecule expressed in T cells, which was reported to induce T cell apoptosis (43). Although most studies on immune evasion by PD-1 have focused on T cells, recent reports have demonstrated an increasing expression of PD-1 on M2 macrophages (44) and the impairing phagocytic ability of PD-1$^+$ M2 macrophages (45). Increasing evidence suggests that targeting macrophages benefits cancer treatment (46, 47). Therefore, these conclusions are consistent with what we observed in this experiment, that is, the frequency of PD-1$^+$ M2 macrophages was higher in cervical cancer tissues than in paracancerous tissue. As the core of immunosuppressive cells and cytokine networks, macrophages play a crucial role in tumor immune evasion. Increasing evidence indicates that potential mechanisms of tumor immune escape mediated by macrophages imply interpretation and breakthrough to the bottleneck of current tumor immunotherapy (48). Our study on aggregation of PD-1$^+$ M2 macrophages might play an important role in immune escape of cervical cancer.

Although the role of PD-1$^+$ M2 macrophages has been clarified, the molecular mechanisms leading to the change of macrophage phenotype and phagocytosis have not been fully studied. Our study goes in depth to reveal the mechanism. Because we found the increase of METTL14 expression and the number of PD-1$^+$ M2 macrophages at the same time, we investigated the potential relevance between them. In our study, we found that the expression of M2-associated genes (CD206) and PD-1 significantly decreased in macrophages that were cocultured with METTL14-deficient cervical cancer cells. In addition, the phagocytotic function of macrophages cocultured with METTL14-deficient cervical cancer cells decreased. Specifically, these results confirm that abnormal METTL14 in cervical cancer tissues is related to function and expression of PD-1 in M2 macrophages, which suggests that METTL14 has a role in TAMs of cervical cancer. Recent studies have suggested that transcripts of key genes of the innate immune system are marked by m6A methyltransferase, which are responsible for the maintenance of innate antiviral responses (49–52) or are essential for dendritic cell activation (53), indicating that the expression of m6A methyltransferase is implicated in innate immune responses. However, macrophages, as an important component of innate immunity, lack the mechanism research related to m6A. Our study addresses that gap and documents that METTL14 overexpression in tumor tissues may increase the expression of PD-1 on the surface of macrophages, thus preventing macrophages from devouring tumor cells. Thus, METTL14 in tumor tissues appears to be necessary for macrophage activation.

To date, the potential molecular mechanism of METTL14 on macrophages is still unknown. A recent study has shown that cancer cells can harness metabolic byproducts to hijack the functions of tumor-infiltrating immune cells to their own benefit (54–56). Therefore, MTLL14 in tumor cells may mediate the TAM subsets through several metabolites (such as NO, fatty acid, and lactic acid). In our experiments, we detected abnormal lactate content in the cocultured cell supernatants, suggesting that lactic acid may participate in the interaction between METTL14 expression and TAMs. To verify the effect of lactic acid, we blocked the stimulation of lactic acid

through inhibiting the expression of GPR81 on the surface of macrophages. Indeed, the inhibition of GPR81 activity resulted in a significant blockade of M2-like TAM phenotypes and the expression of PD-1 on the surface of macrophages. Additionally, the phagocytic function of macrophages also decreased. These results indicate that the change in lactic acid content caused by abnormal METTL14 expression plays a role in regulating macrophage phenotype and function. Previous research has shown that lactic acid and an acidic TME in pancreatic cancer tissues are consistent with the distribution of M2 macrophages (28). In addition, there is still growing evidence to prove that M2 TAMs preferentially accumulate in high-concentration lactic acid in the TME (28, 57–59). Our results go beyond previous reports, showing that lactic acid cannot only affect the polarization of macrophages, but also affect the phagocytosis of macrophages.

Our study also focused on the source of lactic acid that causes changes in macrophage function. It has been demonstrated that glycolysis is the primary source of lactic acid in tumors (60, 61). It is known that glycolysis is associated with an unfavorable prognosis and malignant progression in various human cancers, including cervical cancer (28, 30, 35, 59, 62–67). What caught our attention was that the roles of METTL14 on the tumorous glycolysis are still infrequently reported in existing research. The findings of the current study indicate that metabolic enzymes and transporters involved in glycolysis are expressed more frequently in cervical cancer tissues than in paracancerous tissues. At the same time, our results also revealed that METTL14 increased the level of glycolysis and concentrations of metabolites both in vitro and in vivo. In previous discussion, we have proposed that lactic acid produced by tumorous glycolysis is an effective way to regulate the function and polarization of macrophages. To verify the role of glycolysis, glycolysis inhibitors were added to the coculture system of cervical cancer cells and macrophages. Our results demonstrated that when glycolysis is effectively blocked, the inhibition of phagocytic function of macrophages caused by METTL14 overexpression is relieved. These results indicate that although 2-DG is an effective inhibitor of glycolysis, it still cannot fully rescue the activation of glycolysis caused by high expression METTL14. Overall, our findings at least hint that tumorous glycolysis/lactic acid might be the potential mechanism for the function and polarization of macrophages mediated by METTL14 expression in cervical cancer.

Furthermore, the pathway of METTL14 that regulates glycolysis needs to be studied urgently. AMPK is a metabolic fuel gauge conserved along an evolutionary scale in eukaryotes that senses changes in the intracellular AMP/ATP ratio. In eukaryotic cells, AMPK plays a significant role in regulating the cellular energy balance. Given its vital role in regulating energy balance, AMPK has aroused considerable interest as a potential therapeutic target for metabolic disorders and cancer (68–70). In vivo, various physiological conditions, including mitochondrial inhibition, nutritional deficiency, and exercise, can influence AMPK, which may be induced by regulating ATP/ADP (71). Targeted metabolomics results showed that the reduced expression of METTL14 lead to lower concentrations of ADP. ADP can combine with the CBS structural domain to activate AMPK expression (72). This analysis found evidence for the regulation of AMPK on glycolysis. In this study, we discovered that the abnormal expression of METTL14 inhibited the m6A RNA methylation of AMPK. Furthermore, METTL14 increased AMPK protein expression, thereby accelerating glycolysis, whereas dorsomorphin successfully inhibited the level of glycolysis. After blocking AMPK expression in the METTL14-overexpressed cell lines, the level of glycolysis also changed compared with any univariate group. Collectively, these findings illustrate that AMPK signaling might be a potential mechanism by which METTL14 regulates glycolysis.

Taken together, we confirm the abnormal m6A methylation in cervical cancer and the high expression of the methyltransferase METTL14. METTL14 enhances the level of glycolysis through the AMPK pathway. Abnormal activity of tumorous glycolysis can lead to the accumulation of extracellular lactate acid, which in turn increases the expression of PD-1 in M2 macrophages and inhibits the phagocytosis of macrophages. Collectively, our findings demonstrate that METTL14/glycolysis might be a (to our knowledge) new therapeutic target in cancer treatment. On the one hand, intervention on this target can directly inhibit the growth of cervical cancer; on the other hand, it can enhance the recognition and phagocytosis of macrophages, which could prevent tumors from immune escape. This conclusion has been effectively verified by our experiments in vivo and in vitro. Overall, our results suggest the possibility of developing therapeutic strategies against cancer progression by targeting m6A modification.

Acknowledgments

The visual abstract was created using BioRender.com.

Disclosures

The authors have no financial conflicts of interest.

References

1. Buskwofie, A., G. David-West, and C. A. Clare. 2020. A review of cervical cancer: incidence and disparities. *J. Natl. Med. Assoc.* 112: 229–232.
2. Bhatla, N., and S. Singhal. 2020. Primary HPV screening for cervical cancer. *Best Pract. Res. Clin. Obstet. Gynaecol.* 65: 98–108.
3. Arezzo, F., G. Cormio, V. Loizzi, G. Cazzato, V. Cataldo, C. Lombardi, G. Ingravallo, L. Resta, and E. Cicinelli. 2021. HPV-negative cervical cancer: a narrative review. *Diagnostics (Basel)* 11: 952.
4. Sun, T., R. Wu, and L. Ming. 2019. The role of m6A RNA methylation in cancer. *Biomed. Pharmacother.* 112: 108613.
5. An, Y., and H. Duan. 2022. The role of m6A RNA methylation in cancer metabolism. *Mol. Cancer* 21: 14.
6. Guo, J., J. Zheng, H. Zhang, and J. Tong. 2021. RNA m6A methylation regulators in ovarian cancer. *Cancer Cell Int.* 21: 609.
7. Oerum, S., V. Meynier, M. Catala, and C. Tisné. 2021. A comprehensive review of m6A/m6Am RNA methyltransferase structures. *Nucleic Acids Res.* 49: 7239–7255.
8. Gao, R., M. Ye, B. Liu, M. Wei, D. Ma, and K. Dong. 2021. m6A modification: a double-edged sword in tumor development. *Front. Oncol.* 11: 679367.
9. Wang, Q., X. Guo, L. Li, Z. Gao, X. Su, M. Ji, and J. Liu. 2020. N^6-methyladenosine METTL3 promotes cervical cancer tumorigenesis and Warburg effect through YTHDF1/HK2 modification. *Cell Death Dis.* 11: 911.
10. Li, Z., Y. Peng, J. Li, Z. Chen, F. Chen, J. Tu, S. Lin, and H. Wang. 2020. N^6-methyladenosine regulates glycolysis of cancer cells through PDK4. *Nat. Commun.* 11: 2578.
11. Hu, Y., Y. Li, Y. Huang, Z. Jin, C. Wang, H. Wang, and J. Xu. 2020. METTL3 regulates the malignancy of cervical cancer via post-transcriptional regulation of RAB2B. *Eur. J. Pharmacol.* 879: 173134.
12. Wu, F., Y. Zhang, Y. Fang, S. Ma, H. Zheng, K. Liu, and R. Wang. 2020. Elevated expression of inhibitor of apoptosis-stimulating protein of p53 (iASPP) and methyltransferase-like 3 (METTL3) correlate with poor prognosis in FIGO Ib1-IIa squamous cell cervical cancer. *J. Cancer* 11: 2382–2389.
13. Han, D., J. Liu, C. Chen, L. Dong, Y. Liu, R. Chang, X. Huang, Y. Liu, J. Wang, U. Dougherty, et al. 2019. Anti-tumour immunity controlled through mRNA m^6A methylation and YTHDF1 in dendritic cells. [Published erratum appears in 2019 *Nature* 568: E3.] *Nature* 566: 270–274.
14. Li, H. B., J. Tong, S. Zhu, P. J. Batista, E. E. Duffy, J. Zhao, W. Bailis, G. Cao, L. Kroehling, Y. Chen, et al. 2017. m^6A mRNA methylation controls T cell homeostasis by targeting the IL-7/STAT5/SOCS pathways. *Nature* 548: 338–342.
15. Kuznetsova, T., K. H. M. Prange, C. K. Glass, and M. P. J. de Winther. 2020. Transcriptional and epigenetic regulation of macrophages in atherosclerosis. *Nat. Rev. Cardiol.* 17: 216–228.
16. Klichinsky, M., M. Ruella, O. Shestova, X. M. Lu, A. Best, M. Zeeman, M. Schmierer, K. Gabrusiewicz, N. R. Anderson, N. E. Petty, et al. 2020. Human chimeric antigen receptor macrophages for cancer immunotherapy. *Nat. Biotechnol.* 38: 947–953.
17. Pedraza-Brindis, E. J., K. Sánchez-Reyes, G. Hernández-Flores, A. Bravo-Cuellar, L. F. Jave-Suárez, A. Aguilar-Lemarroy, P. Gómez-Lomelí, B. A. López-López, and P. C. Ortiz-Lazareno. 2016. Culture supernatants of cervical cancer cells induce an M2 phenotypic profile in THP-1 macrophages. *Cell. Immunol.* 310: 42–52.
18. Kawachi, A., H. Yoshida, S. Kitano, Y. Ino, T. Kato, and N. Hiraoka. 2018. Tumor-associated $CD204^+$ M2 macrophages are unfavorable prognostic indicators in uterine cervical adenocarcinoma. *Cancer Sci.* 109: 863–870.

19. Yi, M., X. Zheng, M. Niu, S. Zhu, H. Ge, and K. Wu. 2022. Combination strategies with PD-1/PD-L1 blockade: current advances and future directions. *Mol. Cancer* 21: 28.
20. Yi, M., D. Jiao, H. Xu, Q. Liu, W. Zhao, X. Han, and K. Wu. 2018. Biomarkers for predicting efficacy of PD-1/PD-L1 inhibitors. *Mol. Cancer* 17: 129.
21. Zou, W., J. D. Wolchok, and L. Chen. 2016. PD-L1 (B7-H1) and PD-1 pathway blockade for cancer therapy: mechanisms, response biomarkers, and combinations. *Sci. Transl. Med.* 8: 328rv4.
22. Pardoll, D. M. 2012. The blockade of immune checkpoints in cancer immunotherapy. *Nat. Rev. Cancer* 12: 252–264.
23. Yao, A., F. Liu, K. Chen, L. Tang, L. Liu, K. Zhang, C. Yu, G. Bian, H. Guo, J. Zheng, et al. 2014. Programmed death 1 deficiency induces the polarization of macrophages/microglia to the M1 phenotype after spinal cord injury in mice. *Neurotherapeutics* 11: 636–650.
24. Gordon, S. R., R. L. Maute, B. W. Dulken, G. Hutter, B. M. George, M. N. McCracken, R. Gupta, J. M. Tsai, R. Sinha, D. Corey, et al. 2017. PD-1 expression by tumour-associated macrophages inhibits phagocytosis and tumour immunity. *Nature* 545: 495–499.
25. Ma, L. N., X. B. Huang, K. P. Muyayalo, G. Mor, and A. H. Liao. 2020. Lactic acid: a novel signaling molecule in early pregnancy? *Front. Immunol.* 11: 279.
26. Gardner, D. K. 2015. Lactate production by the mammalian blastocyst: manipulating the microenvironment for uterine implantation and invasion? *BioEssays* 37: 364–371.
27. Henze, A. T., and M. Mazzone. 2016. The impact of hypoxia on tumor-associated macrophages. *J. Clin. Invest.* 126: 3672–3679.
28. Colegio, O. R., N. Q. Chu, A. L. Szabo, T. Chu, A. M. Rhebergen, V. Jairam, N. Cyrus, C. E. Brokowski, S. C. Eisenbarth, G. M. Phillips, et al. 2014. Functional polarization of tumour-associated macrophages by tumour-derived lactic acid. *Nature* 513: 559–563.
29. Goswami, K. K., S. Banerjee, A. Bose, and R. Baral. 2022. Lactic acid in alternative polarization and function of macrophages in tumor microenvironment. *Hum. Immunol.* 83: 409–417.
30. Certo, M., C. H. Tsai, V. Pucino, P. C. Ho, and C. Mauro. 2021. Lactate modulation of immune responses in inflammatory versus tumour microenvironments. *Nat. Rev. Immunol.* 21: 151–161.
31. Ye, H., Q. Zhou, S. Zheng, G. Li, Q. Lin, L. Wei, Z. Fu, B. Zhang, Y. Liu, Z. Li, and R. Chen. 2018. Tumor-associated macrophages promote progression and the Warburg effect via CCL18/NF-kB/VCAM-1 pathway in pancreatic ductal adenocarcinoma. *Cell Death Dis.* 9: 453.
32. Dietl, K., K. Renner, K. Dettmer, B. Timischl, K. Eberhart, C. Dorn, C. Hellerbrand, M. Kastenberger, L. A. Kunz-Schughart, P. J. Oefner, et al. 2010. Lactic acid and acidification inhibit TNF secretion and glycolysis of human monocytes. *J. Immunol.* 184: 1200–1209.
33. Kuo, L. J., and L. X. Yang. 2008. γ-H2AX—a novel biomarker for DNA double-strand breaks. *In Vivo* 22: 305–309.
34. Brown, T. P., and V. Ganapathy. 2020. Lactate/GPR81 signaling and proton motive force in cancer: role in angiogenesis, immune escape, nutrition, and Warburg phenomenon. *Pharmacol. Ther.* 206: 107451.
35. Yang, K., J. Xu, M. Fan, F. Tu, X. Wang, T. Ha, D. L. Williams, and C. Li. 2020. Lactate suppresses macrophage pro-inflammatory response to LPS stimulation by inhibition of YAP and NF-κB activation via GPR81-mediated signaling. *Front. Immunol.* 11: 587913.
36. Manoharan, I., P. D. Prasad, M. Thangaraju, and S. Manicassamy. 2021. Lactate-dependent regulation of immune responses by dendritic cells and macrophages. *Front. Immunol.* 12: 691134.
37. Hoque, R., A. Farooq, A. Ghani, F. Gorelick, and W. Z. Mehal. 2014. Lactate reduces liver and pancreatic injury in Toll-like receptor- and inflammasome-mediated inflammation via GPR81-mediated suppression of innate immunity. *Gastroenterology* 146: 1763–1774.
38. Fang, J., H. Zhang, and S. Jin. 2014. Epigenetics and cervical cancer: from pathogenesis to therapy. *Tumour Biol.* 35: 5083–5093.
39. Chen, M., and C. M. Wong. 2020. The emerging roles of N6-methyladenosine (m6A) deregulation in liver carcinogenesis. *Mol. Cancer* 19: 44.
40. Guan, Q., H. Lin, L. Miao, H. Guo, Y. Chen, Z. Zhuo, and J. He. 2022. Functions, mechanisms, and therapeutic implications of METTL14 in human cancer. *J. Hematol. Oncol.* 15: 13.
41. Shi, Y., Y. Zhuang, J. Zhang, M. Chen, and S. Wu. 2020. METTL14 inhibits hepatocellular carcinoma metastasis through regulating EGFR/PI3K/AKT signaling pathway in an m6A-dependent manner. *Cancer Manag. Res.* 12: 13173–13184.
42. Liu, J., M. A. Eckert, B. T. Harada, S. M. Liu, Z. Lu, K. Yu, S. M. Tienda, A. Chryplewicz, A. C. Zhu, Y. Yang, et al. 2018. m^6A mRNA methylation regulates AKT activity to promote the proliferation and tumorigenicity of endometrial cancer. *Nat. Cell Biol.* 20: 1074–1083.
43. Ishida, Y., Y. Agata, K. Shibahara, and T. Honjo. 1992. Induced expression of PD-1, a novel member of the immunoglobulin gene superfamily, upon programmed cell death. *EMBO J.* 11: 3887–3895.
44. Cai, H., Y. Zhang, J. Wang, and J. Gu. 2021. Defects in macrophage reprogramming in cancer therapy: the negative impact of PD-L1/PD-1. *Front. Immunol.* 12: 690869.
45. Kono, Y., H. Saito, W. Miyauchi, S. Shimizu, Y. Murakami, Y. Shishido, K. Miyatani, T. Matsunaga, Y. Fukumoto, Y. Nakayama, et al. 2020. Increased PD-1-positive macrophages in the tissue of gastric cancer are closely associated with poor prognosis in gastric cancer patients. *BMC Cancer* 20: 175.
46. Du, S., J. Qian, S. Tan, W. Li, P. Liu, J. Zhao, Y. Zeng, L. Xu, Z. Wang, and J. Cai. 2022. Tumor cell-derived exosomes deliver TIE2 protein to macrophages to promote angiogenesis in cervical cancer. *Cancer Lett.* 529: 168–179.
47. Kim, S. Y., S. Kim, J. E. Kim, S. N. Lee, I. W. Shin, H. S. Shin, S. M. Jin, Y. W. Noh, Y. J. Kang, Y. S. Kim, et al. 2019. Lyophilizable and multifaceted Toll-like receptor 7/8 agonist-loaded nanoemulsion for the reprogramming of tumor microenvironments and enhanced cancer immunotherapy. *ACS Nano* 13: 12671–12686.
48. Qiu, Y., T. Chen, R. Hu, R. Zhu, C. Li, Y. Ruan, X. Xie, and Y. Li. 2021. Next frontier in tumor immunotherapy: macrophage-mediated immune evasion. *Biomark. Res.* 9: 72.
49. Liu, Y., Y. You, Z. Lu, J. Yang, P. Li, L. Liu, H. Xu, Y. Niu, and X. Cao. 2019. N^6-methyladenosine RNA modification-mediated cellular metabolism rewiring inhibits viral replication. *Science* 365: 1171–1176.
50. Zheng, Q., J. Hou, Y. Zhou, Z. Li, and X. Cao. 2017. The RNA helicase DDX46 inhibits innate immunity by entrapping m^6A-demethylated antiviral transcripts in the nucleus. [Published erratum appears in 2017 *Nat. Immunol.* 18: 1361.] *Nat. Immunol.* 18: 1094–1103.
51. Wang, L., M. Wen, and X. Cao. 2019. Nuclear hnRNPA2B1 initiates and amplifies the innate immune response to DNA viruses. *Science* 365: eaav0758.
52. Winkler, R., E. Gillis, L. Lasman, M. Safra, S. Geula, C. Soyris, A. Nachshon, J. Tai-Schmiedel, N. Friedman, V. T. K. Le-Trilling, et al. 2019. m^6A modification controls the innate immune response to infection by targeting type I interferons. [Published erratum appears in 2019 *Nat. Immunol.* 20: 243.] *Nat. Immunol.* 20: 173–182.
53. Wang, H., X. Hu, M. Huang, J. Liu, Y. Gu, L. Ma, Q. Zhou, and X. Cao. 2019. Mettl3-mediated mRNA m^6A methylation promotes dendritic cell activation. *Nat. Commun.* 10: 1898.
54. Watson, M. J., and G. M. Delgoffe. 2022. Fighting in a wasteland: deleterious metabolites and antitumor immunity. *J. Clin. Invest.* 132: e148549.
55. Vitale, I., G. Manic, L. M. Coussens, G. Kroemer, and L. Galluzzi. 2019. Macrophages and metabolism in the tumor microenvironment. *Cell Metab.* 30: 36–50.
56. Rawat, D., S. K. Chhonker, R. A. Naik, A. Mehrotra, S. K. Trigun, and R. K. Koiri. 2019. Lactate as a signaling molecule: Journey from dead end product of glycolysis to tumor survival. *Front. Biosci.* 24: 366–381.
57. Shan, T., S. Chen, X. Chen, T. Wu, Y. Yang, S. Li, J. Ma, J. Zhao, W. Lin, W. Li, et al. 2020. M2-TAM subsets altered by lactic acid promote T-cell apoptosis through the PD-L1/PD-1 pathway. *Oncol. Rep.* 44: 1885–1894.
58. Zhou, H. C., W. W. Xin-Yan Yan, X. Q. Yu, X. Y. Liang, Z. C. Du, J. P. Liu, G. H. Long, Zhao, and H. B. Liu. 2022. Lactic acid in macrophage polarization: the significant role in inflammation and cancer. *Int. Rev. Immunol.* 41: 4–18.
59. Zhang, D., Z. Tang, H. Huang, G. Zhou, C. Cui, Y. Weng, W. Liu, S. Kim, S. Lee, M. Perez-Neut, et al. 2019. Metabolic regulation of gene expression by histone lactylation. *Nature* 574: 575–580.
60. Wu, X., L. Qiu, H. Feng, H. Zhang, H. Yu, Y. Du, H. Wu, S. Zhu, Y. Ruan, and H. Jiang. 2022. KHDRBS3 promotes paclitaxel resistance and induces glycolysis through modulated MIR17HG/CLDN6 signaling in epithelial ovarian cancer. *Life Sci.* 293: 120328.
61. Smolle, E., P. Leko, E. Stacher-Priehse, L. Brcic, A. El-Heliebi, L. Hofmann, F. Quehenberger, A. Hrzenjak, H. H. Popper, H. Olschewski, and K. Leithner. 2020. Distribution and prognostic significance of gluconeogenesis and glycolysis in lung cancer. *Mol. Oncol.* 14: 2853–2867.
62. Cascone, T., J. A. McKenzie, R. M. Mbofung, S. Punt, Z. Wang, C. Xu, L. J. Williams, Z. Wang, C. A. Bristow, A. Carugo, et al. 2018. Increased tumor glycolysis characterizes immune resistance to adoptive T cell therapy. *Cell Metab.* 27: 977–987.e4.
63. Chen, F., J. Chen, L. Yang, J. Liu, X. Zhang, Y. Zhang, Q. Tu, D. Yin, D. Lin, P. P. Wong, et al. 2019. Extracellular vesicle-packaged HIF-1α-stabilizing lncRNA from tumour-associated macrophages regulates aerobic glycolysis of breast cancer cells. *Nat. Cell Biol.* 21: 498–510.
64. Kumagai, S., S. Koyama, K. Itahashi, T. Tanegashima, Y. T. Lin, Y. Togashi, T. Kamada, T. Irie, G. Okumura, H. Kono, et al. 2022. Lactic acid promotes PD-1 expression in regulatory T cells in highly glycolytic tumor microenvironments. *Cancer Cell* 40: 201–218.e9.
65. Hermans, D., S. Gautam, J. C. García-Cañaveras, D. Gromer, S. Mitra, R. Spolski, P. Li, S. Christensen, R. Nguyen, J. X. Lin, et al. 2020. Lactate dehydrogenase inhibition synergizes with IL-21 to promote $CD8^+$ T cell stemness and antitumor immunity. *Proc. Natl. Acad. Sci. USA* 117: 6047–6055.
66. de la Cruz-López, K. G., L. J. Castro-Muñoz, D. O. Reyes-Hernández, A. García-Carrancá, and J. Manzo-Merino. 2019. Lactate in the regulation of tumor microenvironment and therapeutic approaches. *Front. Oncol.* 9: 1143.
67. Cheng, A., P. Zhang, B. Wang, D. Yang, X. Duan, Y. Jiang, T. Xu, Y. Jiang, J. Shi, C. Ding, et al. 2019. Aurora-A mediated phosphorylation of LDHB promotes glycolysis and tumor progression by relieving the substrate-inhibition effect. *Nat. Commun.* 10: 5566.
68. Carling, D. 2017. AMPK signalling in health and disease. *Curr. Opin. Cell Biol.* 45: 31–37.
69. Herzig, S., and R. J. Shaw. 2018. AMPK: guardian of metabolism and mitochondrial homeostasis. *Nat. Rev. Mol. Cell Biol.* 19: 121–135.
70. Li, Y., and Y. Chen. 2019. AMPK and autophagy. *Adv. Exp. Med. Biol.* 1206: 85–108.
71. Gowans, G. J., and D. G. Hardie. 2014. AMPK: a cellular energy sensor primarily regulated by AMP. *Biochem. Soc. Trans.* 42: 71–75.
72. Steinberg, G. R., and D. G. Hardie. 2023. New insights into activation and function of the AMPK. *Nat. Rev. Mol. Cell Biol.* 24: 255–272.